A MICROSCOPIC APPROACH TO PEDESTRIAN DYNAMICS AND THE ONSET OF DISEASE SPREADING

A Dissertation Presented to
the Faculty of the Department of Mathematics
University of Houston

In Partial Fulfillment
of the Requirements for the Degree
Doctor of Philosophy

By
Krithika Rathinakumar
May 2019

A MICROSCOPIC APPROACH TO PEDESTRIAN DYNAMICS AND THE ONSET OF DISEASE SPREADING

Krithika Rathinakumar

APPROVED:

Dr. Annalisa Quaini, Committee Chair

Dr. William Fitzgibbon

Dr. Ilya Timofeyev

Dr. LieJune Shiau
University of Houston - Clear Lake

Dr. Dan E. Wells, Dean, College of Natural Sciences and Mathematics

Acknowledgements

I would like to express my deep gratitude to Dr. Annalisa Quaini for being the most supportive advisor one could ask for. Her patient guidance, encouragement and belief in me has helped me both in this research work and with my academic life at UH.

I convey my gratitude to Dr. William Fitzgibbon, whose valuable inputs helped me expand the scope of my work. I would also like to thank my committee members: Dr. William Fitzgibbon, Dr. Ilya Timofeyev and Dr. LieJune Shiau for their support and feedback.

I thank the Department of Mathematics, University of Houston for all the resources that were provided to me, which greatly helped me in my work.

I thank my brother Sivashankar, who motivated me to consider a Ph.D in the first place and helped me settle into life at Houston. Without him, its hard to imagine where I would be right now!

Thanks to my parents, Jothimani and Rathinakumar, and sister Radha for keeping me sane through the last few years. Our conversations everyday always kept me high-spirited. I also wish to thank my parents-in-law Veena and Ramanathan, and sister-in-law Rohini, whose periodic enquiries on the progress of my work have kept me motivated and energized.

Thanks to my friends: Vardini, OPUS, Sabrine, Dipa, Prajakta and fellow Qties: Daewa and Kayla, for motivating and encouraging me throughout the years.

Finally, I am grateful for my husband Gokul, for being my rubber duck whenever I needed one.

A MICROSCOPIC APPROACH TO PEDESTRIAN DYNAMICS AND THE ONSET OF DISEASE SPREADING

An Abstract of a Dissertation

Presented to

the Faculty of the Department of Mathematics

University of Houston

In Partial Fulfillment

of the Requirements for the Degree

Doctor of Philosophy

By

Krithika Rathinakumar

May 2019

Abstract

In this dissertation we analyze the numerical results of a microscopic approach that models pedestrian dynamics.

Firstly, we focus on a space-continuous model that represents pedestrian dynamics by the forces acting on them. We consider that each pedestrian is driven by the desire to reach a certain target and is influenced by the space geometry as well as by the pedestrians surrounding them. These forces on the pedestrians are modeled using Newton's second law of dynamics as a guiding principle. The model results in a high-dimensional system of second order ordinary differential equations. The time evolution of the positions and velocities of all pedestrians is then obtained by numerical integration.

The various parameters in our model are numerically calibrated for a simple straight corridor and their significance to the model is analyzed. A major side effect of spatially continuous models are oscillations and overlaps. They are also analyzed in a quantitative manner for the same corridor.

Next, we validate our model through a serious of experiments. We compute the evacuation time from a room with varying exit door size. Our results are compared to the numerical results obtained for the same experiment using a kinetic theory approach. We notice that our model had a higher rate of decrease of evacuation times compared to the kinetic model. Then, we validate our model by comparing with empirical results. We compare the average velocity against the mean density of a group of people passing through a particular portion of a corridor. Our results are in good agreement with the empirical ones. Finally, we show that our model can reproduce self-organization of the pedestrians. We consider a bidirectional flow of pedestrians in a corridor and successfully observe that our model reproduces lane formation without explicitly setting the model to do so.

Lastly, we combine our pedestrian dynamics model with a contact tracking model to compute the average number of people getting infected by sick people inside airports.

Contents

Chapter 1

Introduction

Lately, the study of pedestrian dynamics has gained much interest from researchers of various scientific fields. Research on this topic began with empirical observations in 1950s to produce efficient architectural designs for public places, then moved on to simulating pedestrian traffic flow to best analyze panic situations that might require evacuations [27, 58]. In more recent years, the computational and analytical features related to existing models garnered interest from applied mathematicians and physicians, since many models were becoming reliable in simulating pedestrian flows. Such successful dynamic models help in building safer structures (optimal evacuation during a panic situation), controlling crowds during mass events, controlling the spread of an infectious disease in its initial stages by contact tracing, and so on.

In this paper, we analyze one such application of modeling pedestrian dynamics - contact tracing. Contact tracing is a potentially powerful disease control strategy in which the people who were in close contact to infectious persons are traced. These traced people are then monitored so that if they become symptomatic, they can be efficiently isolated, resulting in reduced transmissions [22, 24].

Contact tracing recently gained public attention because of its importance as a control strategy in the $2014-2015$ Ebola outbreaks [21, 47, 52]. Direct measurement of the impact of contact tracing on an outbreak has also been recently considered in relation to tuberculosis [26], but a general modeling framework for measuring the population-level effect of contact tracing is needed for other emerging pathogens. As contact tracing aims to identify all potential transmission routes, it suffers from network definition issues; in addition, it is time consuming and relies on individuals providing complete and accurate data about personal relationships.

Previous works about contact tracing have used a range of modeling methods from individual based models on specific networks to compartmental ordinary differential equations at the population level. See [44, 36, 39, 5, 14]. Many differential equation models have incorporated contact tracing implicitly [3, 47], though [35] considered it as a deterministic model with explicit contact tracing for HIV: a different setting than an emerging outbreak.

Standard epidemic theory models describe the number of individuals (or proportion of the population) that are susceptible (S) to, exposed (E) to, infected (I) with and recovered (R) from a particular disease. This classification leads to neglecting various details about the progression of infection. However, the simplification has only led to successful results so far. The SIR and SIS models are the foundation of almost all of mathematical epidemiology. The SIR model is appropriate for infectious diseases that confer lifelong immunity, such as measles or whooping cough [38, 48]. The SIS model is predominantly used for sexually transmitted diseases, such as chlamydia or gonorrhea, where repeat infections are common [33, 25].

The focus of our work is on the initiation of disease spread in a medium size population with a small number of infectious people. Thus, we use the contact tracing model as a network evaluation device by tracking only the number of people who could potentially be infected by sick people around them. Keeping this in mind, we choose a pedestrian dynamics model that can be expanded to track the onset of disease spreading.

Throughout the years different approaches to model pedestrian dynamics have been used. Depending on the scale of the model they can be categorized as macroscopic, microscopic and stochastic [10]. The macroscopic approach is used when crowd dynamics is modeled as a continuum medium characterized by averaged quantities such as mass density and mean velocity [34, 51]. As macroscopic models consider pedestrian flow as a whole, they are used in situations where human interactions are not closely studied. Thus, this approach is not suited for our purpose.

The microscopic approach can be further categorized as discrete or grid-based and continuous or grid-free models. A very popular model belonging to the grid-based category is the Cellular Automata (CA) model [13, 12, 11, 20, 56]. This describes phenomena in space-time by assigning discrete states to a grid of space-cells. These cells can be occupied by a pedestrian or be empty. The movement of pedestrians in space is implemented by passing them from cell to cell (discrete space) in discrete time.

Space-continuous or grid-free models determine the continuous movement of pedestrians based on forces acting on them. Each pedestrian tries to reach a certain target and is influenced by the space geometry as well as by the actual states and positions of the other individuals. The forces acting on people are not only physical but also social [31]. These grid-free microscopic models, also called force-based models, are one of the most popular modeling paradigms of continuous models because they describe the movement of pedestrians well qualitatively. See, e.g., [28, 31, 32, 54, 45, 17, 60, 41] and references therein. Collective phenomena, like unidirectional or bidirectional flow in a corridor [43, 53, 57], lane formation [31, 29, 58], oscillations at bottlenecks [31, 29], the faster-is-slower effect [40, 46], emergency evacuation from buildings [29, 58, 42], are well reproduced. Other advantages of these methods are the ease of implementation, and in particular parallel implementation, and the fact that they permit higher resolution of geometry and time.

Implementations of these models often require additional elements to guarantee realistic behavior, especially in high density situations. Force-based models can be extended into agent based models by incorporating individual features. See, e.g., [19, 15, 4, 2, 6] and references therein. Agent-based models allow for flexibility, extensibility, and capability to realize heterogeneity in crowd dynamics. Both force-based and agent-based models may introduce artifacts due to the force representation of human behavior, leading to unrealistic backward movement or oscillating trajectories. These artifacts can be reduced by incorporating extra rules and/or by elaborate calibrations, at the price of increasing the computational cost.

The third approach is based on the kinetic theory/stochastic description. This scale of observation here is between those of the previous two approaches. In a framework close to that of the kinetic theory of gases, this approach derives a Boltzmann-type evolution equation for the statistical distribution function of the position and velocity of the pedestrians. The kinetic theory approach was introduced in [9] and further developed in [7]. In these papers, the model is valid in unbounded domains. The extension to bounded domains is presented in [1]. Further literature review on this approach can in found in [8].

Most of the references cited so far have been shown to replicate various cases of pedestrian movement qualitatively through analysis and/or numerical simulations.

Obviously, if a model cannot represent a certain phenomenon qualitatively, there is no hope for any quantitative agreement between model prediction and practical experiments. However before using a model for quantitative predictions, the model itself must be validated and the numerical method used to implement the model must be verified [23]. A verified method is capable of correctly solving the problem equations, while a valid model is able to correctly describe the features of the problem (i.e., it uses the right equations). Validation of pedestrian flow models are complicated by the lack of reliable experimental data. In addition, the few available datasets show large differences [49, 50, 59]. In order to make the models more reliable, evolutionary adjustment of the parameters and data assimilations have also been proposed in [55, 37] respectively.

As stated earlier, the focus of this work is on the initiation of disease spread. A small number of infected people are introduced into a given environment like an airport, where a disease spread initiation could occur. Small to intermediate number of interactions occur between the pedestrians inside this environment. As most currently used models in epidemiology cannot handle these scenarios, we model the pedestrian dynamics using a grid-free microscopic approach, in particular, the force-based approach. We then apply a 'tracking' part to the model to track the disease spread. First, we concentrate on the pedestrian dynamics model, then we trace the disease spread.

Force-based models contain free parameters that can be adequately calibrated to achieve a good quantitative description. However, depending on the simulated geometry, the set of parameters often changes. In most works, quantitative investigations of pedestrian dynamics were restricted to a specific scenario or geometry, see. [18]. The pedestrian dynamics model is taken from [18]. We first calibrate the model for pedestrian motion in corridors. We then validate the model by comparing the results obtained by our model with a kinetic model in [1] and with empirical results in [59]. Finally, we observe the self-organized lane formation of pedestrian dynamics in normal situations.

Next, we add the 'track' part to that model to track the disease spread. This updated microscopic model is used to analyze the initial disease spread in airports. The sick people in the system are referred to as primary contacts and the people infected by the primary are called secondary contacts. For our contact tracing model, we consider a simple, explicit approach by introducing a sickness domain (a circle, for simplicity) around a primary contact. A healthy but vulnerable person who is in that sickness circle for a certain amount of time may get infected and become a secondary contact. Finally, using the combined model, we calculate the average number of secondary contacts produced in an environment.

The outline of this dissertation is as follows.

In **Chapter 2**, we introduce the problem definition for the microscopic modeling of pedestrian dynamics. The force - based mathematical model is set up and its advantages and disadvantages are discussed. Then, the numerical method for the model is described.

In **Chapter 3**, we calibrate the parameters of the model. Each parameter of the model is numerically analyzed to see its effect on the model.

In **Chapter 4**, we validate the model by comparing it with numerical experiments that use a kinetic theory approach and with empirical results. In this chapter, we also show that the model reproduces self-organization of pedestrians.

In **Chapter 5**, we present the contact tracking model used along with the pedestrian dynamic model to trace the initial spread of an airborne disease. We also show the numerical results for the contact tracking model. Sick people who board an airplane and reach their destination by passing through a transit airport are traced. The numerical simulations are used to predict the average number of people that could get infected.

Chapter 2

Mathematical Model and Numerical Method

2.1 Introduction

A microscopic grid free (force based) approach is considered for modeling pedestrian dynamics. These models use Newton's second law of motion as a guiding principle. Each pedestrian walks towards a target and their motion is influenced by other pedestrians and space geometry. A pedestrian in the model is represented as a circle with varying radius which depends on the pedestrian speed at a particular time. Avoiding overlapping between pedestrians and oscillations in their trajectories is difficult to accomplish in force based models. Increasing the strength of an interaction force with the aim of excluding overlapping during simulations leads to oscillations in the trajectories of pedestrians. Consequently, backward movements occur in high density situations. Reducing the strength of the interaction force to avoid oscillations leads inevitably to overlapping between pedestrians or between pedestrians and obstacles.

One has to find an adequate value for the strength of the interaction force in order to avoid unrealistic motion [18]. A drawback of representing people as circles is the rotational symmetry, i.e. they occupy the same amount of space in all directions. Representing a person as an ellipse is closer to the projection of required space for a human on the plane, including the extent of the legs during motion and the lateral swaying of the body. Ellipses seem to be superior to circles for low and medium values of the density but we stick to representing the pedestrians in our model as circles for now as using them posed no disadvantage to our case.

2.2 Mathematical Model

Let us consider a group of N pedestrians in a bounded geometry Ω. Each pedestrian is modeled as a circular disk with a given radius. The dynamics of each pedestrian over a time interval of interest $(0, T]$ is modeled using Newton's second law, i.e. for pedestrian i with mass m_i and center of mass at $\boldsymbol{r}_i$ the law of motion is:

$$m_i \ddot{\boldsymbol{r}}_i = \boldsymbol{f}_i, \quad i = 1, \ldots, N, \tag{2.1}$$

where $\boldsymbol{f}_i$ represents the total forces acting on the pedestrian. Source term $\boldsymbol{f}_i$ includes the force driving the pedestrian toward his/her target and the repulsive forces acting on pedestrian from other pedestrians, and from walls and other obstacles, to prevent collisions and overlapping. The complexity of model (2.1) lies in finding an appropriate description of $\boldsymbol{f}_i$.

We define the set of all pedestrians that influence the motion of pedestrian i at a certain time $t \in (0, T]$ as:

$$\mathcal{P}_i = \{j \in \mathbb{N}, j \leq N \ : \ ||\boldsymbol{r}_j - \boldsymbol{r}_i|| \leq r_p\},$$

where $||||$ denotes the Euclidean norm in $\mathbb{R}^2$ and r_p is a cutoff radius for pedestrian-pedestrian interaction. Given $h > 0$, the boundary $\partial\Omega$ is represented as a set of N_b points: $\mathcal{B} = \{\boldsymbol{r}_k \in \partial\Omega\}_{k=0}^{N_b}$ with $||\boldsymbol{r}_{k+1} - \boldsymbol{r}_k|| = h$, for $k = 0, \ldots, N_b - 1$. The set of boundary points acting on pedestrian i at time $t \in (0, T]$ is:

$$\mathcal{B}_i = \{j \in \mathbb{N}, j \leq N_b : \boldsymbol{r}_j \in \mathcal{B} \text{ and } ||\boldsymbol{r}_j - \boldsymbol{r}_i|| \leq r_w\}$$

where r_w is a cutoff radius for pedestrian-wall interaction. We assume that the total forces $\boldsymbol{f}_i$ consist of three contributions:

$$\boldsymbol{f}_i = \boldsymbol{f}_i^{tar} + \sum_{j \in \mathcal{P}_i} \boldsymbol{f}_{ij}^{ped} + \sum_{j \in \mathcal{B}_i} \boldsymbol{f}_{ij}^{bou}, \quad i = 1, \ldots, N, \tag{2.2}$$

where $\boldsymbol{f}_i^{tar}$ is the force driving pedestrian i to his/her target, $\boldsymbol{f}_{ij}^{ped}$ is the repulsive force pedestrian j exerts on pedestrian i, and $\boldsymbol{f}_{ij}^{bou}$ is the repulsive force due to the domain boundary. Pedestrians try to avoid collisions and contact with other pedestrians and boundary (i.e., wall and objects) by changing their direction. The repulsive forces $\boldsymbol{f}_{ij}^{ped}$ and $\boldsymbol{f}_{ij}^{bou}$ model this attempt to avoid contact.

The driving force models the intention of a pedestrian to move to some destination and walk with a certain desired speed $\overline{v}_i$:

$$\boldsymbol{f}_i^{tar} = m_i \frac{\overline{v}_i \boldsymbol{e}_i - \boldsymbol{v}_i}{\tau}, \tag{2.3}$$

where $\boldsymbol{e}_i$ is the unit vector directed from pedestrian i to his/her target, $\boldsymbol{v}_i = \dot{\boldsymbol{r}}_i$ is the velocity of pedestrian i, and τ is a time constant. For complicated paths, we generate a sequence of "checkpoints" along the path and for each checkpoint j we specify a radius r_j. Checkpoint j is considered to be reached when the pedestrian is within a distance r_j of it. Once the path is assigned to a pedestrian, the target is the first checkpoint along the path and when the first checkpoint is reached the target is updated to the second checkpoint, and so on.

In order to define repulsive force $\boldsymbol{f}_{ij}^{ped}$ in (2.2) we need to introduce some notation. The vector connecting pedestrian i with pedestrian j, directed from i to j, and the corresponding unit vector are denoted by:

$$\boldsymbol{r}_{ij} = \boldsymbol{r}_j - \boldsymbol{r}_i, \quad \boldsymbol{e}_{ij} = \frac{\boldsymbol{r}_{ij}}{||\boldsymbol{r}_{ij}||}.$$

We assume that pedestrian i has an effective diameter d_i that depends linearly on his/her velocity:

$$d_i(\boldsymbol{v}_i) = d_i^0 + \tau_d||\boldsymbol{v}_i||, \tag{2.4}$$

d_i^0 being his/her diameter at rest and τ_d being a proportionality parameter. Eq. (2.4) accounts for the fact that a faster pedestrian has an effective larger diameter since he/she will keep obstacles and other pedestrians at a larger distance. The effective distance between pedestrians i and j is then:

$$d_{ij} = \|\boldsymbol{r}_{ij}\| - \frac{1}{2}(d_i(\boldsymbol{v}_i) + d_j(\boldsymbol{v}_j)). \tag{2.5}$$

We can now write the repulsive force as:

$$\boldsymbol{f}_{ij}^{ped} = -m_i k_{ij} \frac{(\mu \bar{v}_i + v_{ij})^2}{d_{ij}} \boldsymbol{e}_{ij}, \tag{2.6}$$

where μ is a parameter used to tune the strength of the force, v_{ij} is the component of the velocity of i relative to j in the direction of $\boldsymbol{e}_{ij}$:

$$v_{ij} = \frac{1}{2}\left[(\boldsymbol{v}_i - \boldsymbol{v}_j)\cdot\boldsymbol{e}_{ij} + \left|(\boldsymbol{v}_i - \boldsymbol{v}_j)\cdot\boldsymbol{e}_{ij}\right|\right] = \begin{cases} (\boldsymbol{v}_i - \boldsymbol{v}_j)\cdot\boldsymbol{e}_{ij} & \text{if } (\boldsymbol{v}_i - \boldsymbol{v}_j)\cdot\boldsymbol{e}_{ij} > 0, \\ 0 & \text{otherwise,} \end{cases} \tag{2.7}$$

and k_{ij} is a coefficient that reduces the action-field of the repulsive force to the angle of vision of each pedestrian (i.e., 180°):

$$k_{ij} = \frac{1}{2}\frac{\boldsymbol{v}_i\cdot\boldsymbol{e}_{ij} + |\boldsymbol{v}_i\cdot\boldsymbol{e}_{ij}|}{\|\boldsymbol{v}_i\|} = \begin{cases} \frac{\boldsymbol{v}_i\cdot\boldsymbol{e}_{ij}}{\|\boldsymbol{v}_i\|} & \text{if } \boldsymbol{v}_i\cdot\boldsymbol{e}_{ij} > 0 \text{ and } \|\boldsymbol{v}_i\| \neq 0, \\ 0 & \text{otherwise.} \end{cases} \tag{2.8}$$

As is intuitive, the repulsive force in (2.6) is directed in the opposite direction of $\boldsymbol{e}_{ij}$ and its modulus is inversely proportional to the effective distance between pedestrians i and pedestrian j. Moreover, the strength of the repulsive force $\boldsymbol{f}_{ij}^{ped}$ depends on the angle between $\boldsymbol{v}_i$ and $\boldsymbol{e}_{ij}$. In fact, the coefficient k_{ij} takes its maximum value (i.e., 1) when pedestrian i is moving in the same direction as $\boldsymbol{e}_{ij}$ and it takes its minimum value (i.e., 0) when the angle between $\boldsymbol{v}_i$ and $\boldsymbol{e}_{ij}$ is bigger than 90°. Notice that, thanks to the definition of v_{ij}, pedestrian i feels the repulsive force due to pedestrian j only if they are moving toward each other. So, e.g., if pedestrian j is close to pedestrian i, but faster than and ahead of i, then $\boldsymbol{f}_{ij}^{ped} = \mathbf{0}$.

The term $\mu \overline{v}_i$ at the numerator in eq. (2.6) prevents collisions due to an unacceptably small repulsive force when the distance between the two pedestrian is small and the relative speed is low. This is motivated by the observation that pedestrians with a large desired speed v_i^0 need stronger repulsive forces to avoid collisions. The case $\mu = 0$ corresponds to the centrifugal force model introduced in [58], which is known to lead to realistic results only if supplemented with a collision detection technique. See also [16] for details.

In order to define $\boldsymbol{f}_{ij}^{bou}$, we note that the repulsive force between a pedestrian i and a wall is zero if i is walking parallel to the wall. In the model though, this is not enough to avoid very small repulsive forces when the pedestrians walks almost parallel to the wall. For this reason, we assume that each pedestrian i feels the repulsive action of three points lying on the boundary: the closest boundary point to pedestrian i denoted by $\boldsymbol{r}_k$, ad the two neighboring points $\boldsymbol{r}_{k-1}$ and $\boldsymbol{r}_{k+1}$ provided that $||\boldsymbol{r}_k - \boldsymbol{r}_i|| \leq r_w$. If indeed $||\boldsymbol{r}_k - \boldsymbol{r}_i|| \leq r_w$, then $\mathcal{B}_i = \{\boldsymbol{r}_{k-1}, \boldsymbol{r}_k, \boldsymbol{r}_{k+1}\}$, otherwise $\mathcal{B}_i = \emptyset$. We assume that the repulsive force exerted by boundary point $j \in \mathcal{B}_i$ on pedestrian i is defined by:

$$\boldsymbol{f}_{ij}^{bou} = -m_i k_{ij} \frac{(\mu_w \overline{v}_i + v_i^n)^2}{d_{ij}^{bou}} \boldsymbol{e}_{ij}, \tag{2.9}$$

where k_{ij} is defined by eq. (2.8), v_i^n is the component of the velocity normal to the boundary and

$$d_{ij}^{bou} = \|\boldsymbol{r}_{ij}\| - \frac{1}{2} d_i(\boldsymbol{v}_i).$$

Thus the mathematical model is complete with the Eqs. (2.1), (2.2), (2.3), (2.6), (2.9).

2.3 Numerical Method

2.3.1 Introduction

Now that the mathematical model for pedestrian motion has been defined, we describe the numerical method that we will implement for the simulations. Model Eqs. 2.1, 2.2, 2.3, 2.6, 2.9 are discretized in time and we start off by calibrating the free parameters τ, d_i^0, τ_d, r_p and r_w of our model to a simple geometry - a corridor. Special focus is on calibrating the interaction constant μ. Once the parameter values are set we move on to validating the model. Two experiments are conducted - one taken from empirical study [59] and another from reference [1]. An experiment from [30] is also conducted to observe a self organizing behavior of pedestrian motion, i.e. lane formation.

2.3.2 Time discretization

We introduce the time-discretization step $\Delta t > 0$ and set $t^n = n\Delta t$, for $n = 1, \dots, N_t$, with $N_t = T/\Delta t$. Moreover, we denote by y^n the approximation of a generic quantity y at the time t^n.

Each pedestrian i, with $i = 1, \ldots, N$, is assigned an initial position $\boldsymbol{r}_i^0$ and an initial velocity v_i^0. The position at time t^{n+1}, with $n \geq 0$ is found with the following centered finite difference approximation of eq. (2.1):

$$m_i \frac{\boldsymbol{r}_i^{n+1} - 2\boldsymbol{r}_i^n + \boldsymbol{r}_i^{n-1}}{\Delta t^2} = \boldsymbol{f}_i^n, \quad n = 0, \ldots, N_t - 1, i = 1, \ldots, N, \tag{2.10}$$

where $\boldsymbol{f}_i^n$ is an approximation of $\boldsymbol{f}_i$ in eq. (2.2) at time t^n. Notice that for $n = 0$ in eq. (2.10) we need $\boldsymbol{r}_i^{-1}$, which is computed as follows:

$$\boldsymbol{r}_i^{-1} = \boldsymbol{r}_i^0 - \Delta t \boldsymbol{v}_i^0, \quad i = 1, \ldots, N.$$

The velocity of each pedestrian at time t^{n+1} is computed by:

$$\boldsymbol{v}_i^{n+1} = \frac{\boldsymbol{r}_i^{n+1} - \boldsymbol{r}_i^n}{\Delta t}, \quad i = 1, \ldots, N. \tag{2.11}$$

Code Implementation: The numerical simulations are implemented in MATLAB and are run on a shared 40-core computing server with 512 GB RAM. Each simulation starts by initializing the pedestrian positions, velocities and paths. At each time step, the new position of all the pedestrians are computed based on the forces acting on them. The pedestrian velocity is then updated using this new position.

Chapter 3

Calibration

3.1 Introduction

The mathematical model described in Sec. 2.2 depends on several parameters. It is necessary to understand how to calibrate these parameters, in particular τ, d_i^0, τ_d and the cutoff radii r_p and r_w, in order to obtain a realistic pedestrian dynamics. Moreover, it is important to check the sensitivity of the model to these parameter values. With this in mind we conduct a series of experiments by varying the parameters. We consider the domain Ω to be a straight corridor. The goal of each experiment is to make a group of pedestrians pass through this corridor as evenly as people would normally do.

We set Ω to be a straight corridor of length 8 m and uniform width 1.8 m. We take a group of $N = 12$ people and simulate their passage through the corridor. As we are interested in understanding the role of all the parameters in the model the size of the group is set to be small. In a large group of pedestrians, the interaction forces become dominant and we would be unable to see the effects of changing the

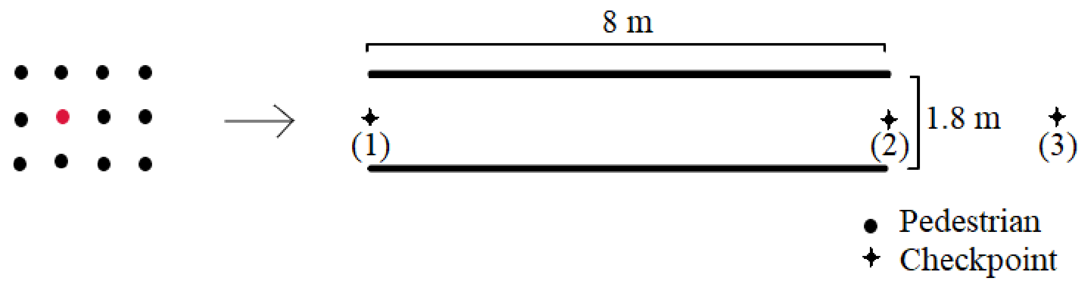

Figure 3.1: A schematic diagram of the straight corridor used for the calibration tests. Here, • represents a pedestrian and • is the pedestrian X whose magnitude of the velocity is considered for the sensitivity analysis.

target force parameters. Initially, the pedestrians are placed 4 m to the left of the corridor, as shown in Fig. 3.1, and they are placed 1 m apart from each other. The people are also initially at rest, i.e. $\boldsymbol{v}_i^0 = \mathbf{0}$ for $i = 1, \ldots, N$. Every pedestrian is assigned the same path : checkpoint 1, then to 2 and finally 3. The width of the corridor 1.8 m is set as the radius associated with each of these checkpoints. Each pedestrian is assigned a desired speed $\overline{v}_i$. The desired speed of all pedestrians are Gaussian distributed with mean 1.55 m/s and standard deviation 0.18 m/s [59]. The simulation is run for $T = 13$s, the time it takes all the pedestrians in the system to exit the corridor. We discretize this time interval $[0, T]$ with time step $\Delta t = 0.01$ s. For all the following tests we compare the magnitude of the velocity (speed) of the pedestrian marked in red in Fig. 3.1 against time. We refer to that pedestrian as pedestrian X. Pedestrian X was chosen as other pedestrians surround X on all sides and thus his/her dynamics certainly depends on all the forces in the model.

Let us start by setting all the model parameters according to [18]: $\tau = 0.5$ s, $\tau_d = 0.53$ s, $r_p = r_w = 2$ m, $d_i^0 = 0.18$ m, and $\mu = \mu_w = 0.2$.

We consider our simulation to be unstable if either of the following happens.

- The pedestrian's current speed exceeds its desired speed.

- Overlaps and oscillations occur.

When the simulation is run with these parameters we notice that some of the pedestrians attain speed greater than their desired speed. In that case the driving force becomes negative and makes the intention of the pedestrian to move in the direction opposite to their destination (driving force becomes a repulsive force). Thus the system is unstable. Furthermore, if the pedestrian speed (which is greater than the desired speed) keeps on increasing, there will eventually be a sudden burst in the motion of the pedestrian causing unrealistic motion. This behavior occurs in our simulation if the parameters are set as above. We also observe the occurrence of pedestrian-pedestrian and pedestrian-wall overlaps for a large amount of time during the run. Thus, we need to find better values for the model parameters.

3.2 Sensitivity Analysis of Model Parameters

The first issue we deal with is the speed of pedestrians becoming greater than their desired speed. From eq. (2.4) we can see that the effective diameter is directly affected by the speed of a pedestrian and that the proportionality parameter τ_d controls this influence of the speed on the effective diameter. As a result we choose to check the sensitivity with respect to τ_d first. The desired speeds of each pedestrian in this run are retained for all the subsequent runs.

Sensitivity to τ_d : Fig. 3.2 displays the speed of pedestrian X for $t \in [0, 13]$ s and three different values of $\tau_d = 0$, 0.10, 0.20 s. We notice that before $t = 1$ s the value of τ_d has little influence on the pedestrian dynamics. This can be explained by fact that τ_d is a proportionality parameter that multiplies the velocity magnitude.

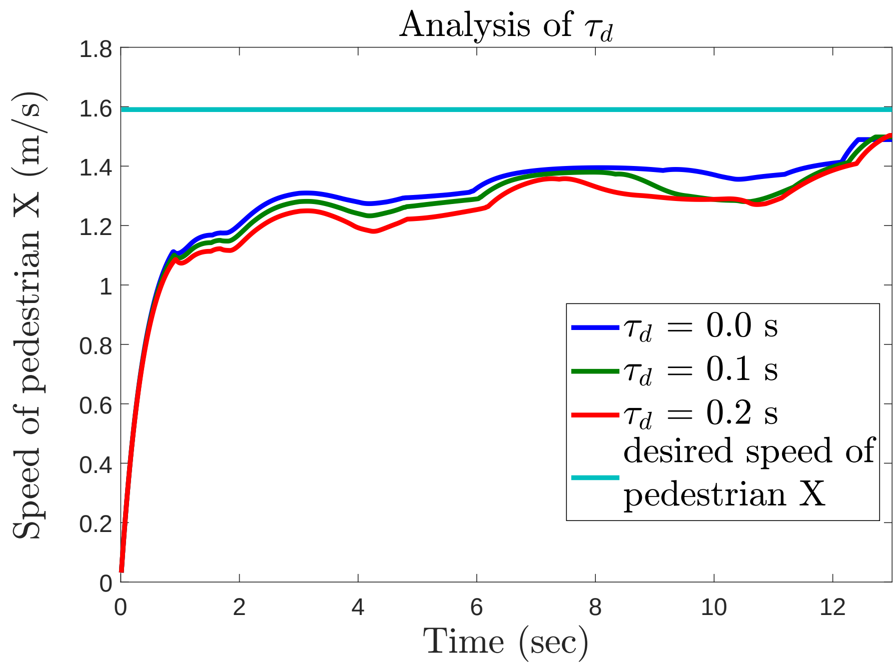

Figure 3.2: Speed of the pedestrian X against time for different values of τ_d.

For small velocity magnitude and small d_i^0 the effective diameter $d_i(\boldsymbol{v}_i)$ is small too. Moreover, till $t = 1$ s the effective distances between pedestrians are large because of the initial positions and the small effective diameters of pedestrians. Thus the interaction forces eq. (2.6) acting on the pedestrians are negligible. The only force in play till $t = 1$ s is the target force $\boldsymbol{f}_i^{tar}$ which is independent of τ_d. After $t = 1$ s, all the forces come into play and hence the pedestrian dynamics is now affected by the value of τ_d. In particular, we notice that the local maxima and minima of speed, while occurring at the same time, decrease as τ_d gets larger. This is due to the fact that τ_d is inversely proportional to both the repulsive forces. Thus the rate at which the speed increases is higher for lower values of τ_d. Overall pedestrian X walks towards the end of the corridor with a speed that never exceeds his/her desired speed (1.59 m/s), as expected. The local minima of speed in the plot occurs due to

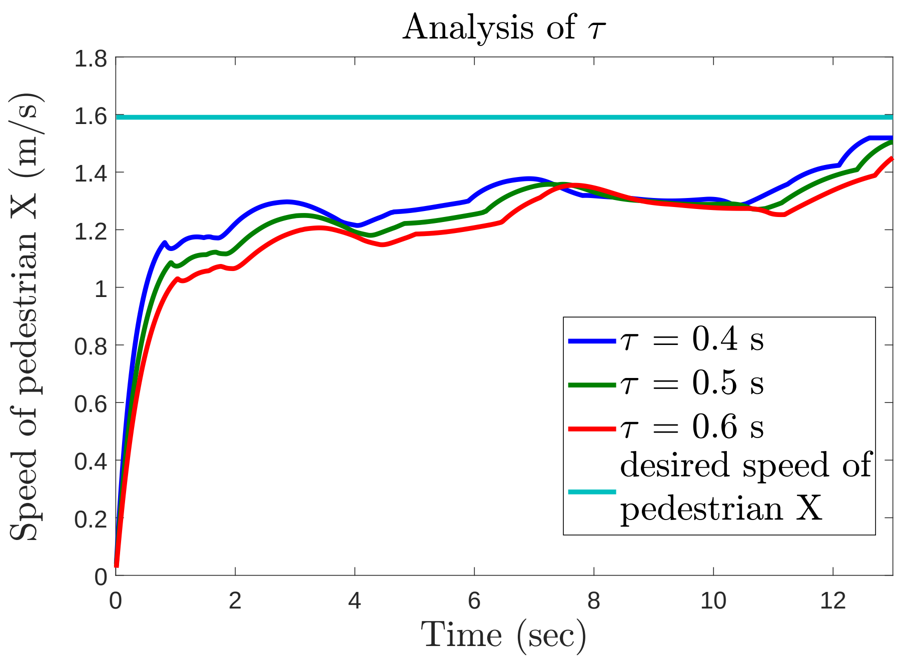

Figure 3.3: Speed of pedestrian X against time for different values of τ.

the interaction with other pedestrians and walls.

Higher values of τ_d were not chosen as for this particular set of desired goal speeds the system became unstable with the speed of some pedestrians exceeding their desired speed. As $\tau_d = 0.20$ s is the highest value for which the system stays stable we fix $\tau_d = 0.20$ s for the upcoming tests. We consider the model parameter τ to be analyzed next.

Sensitivity to τ : In Fig. 3.3 we report the speed of pedestrian X over a time interval of 13 s for three different values of $\tau = 0.4, 0.5, 0.6$ s. We notice that for all the values of τ the magnitude of velocity increases up to a local maximum, decreases to a local minimum, and then oscillates towards the desired speed. As the value of τ gets larger, the values of the local maxima and minima decrease and are reached at a later time. This is as a result of the target force $\boldsymbol{f}_i^{tar}$ being inversely proportional

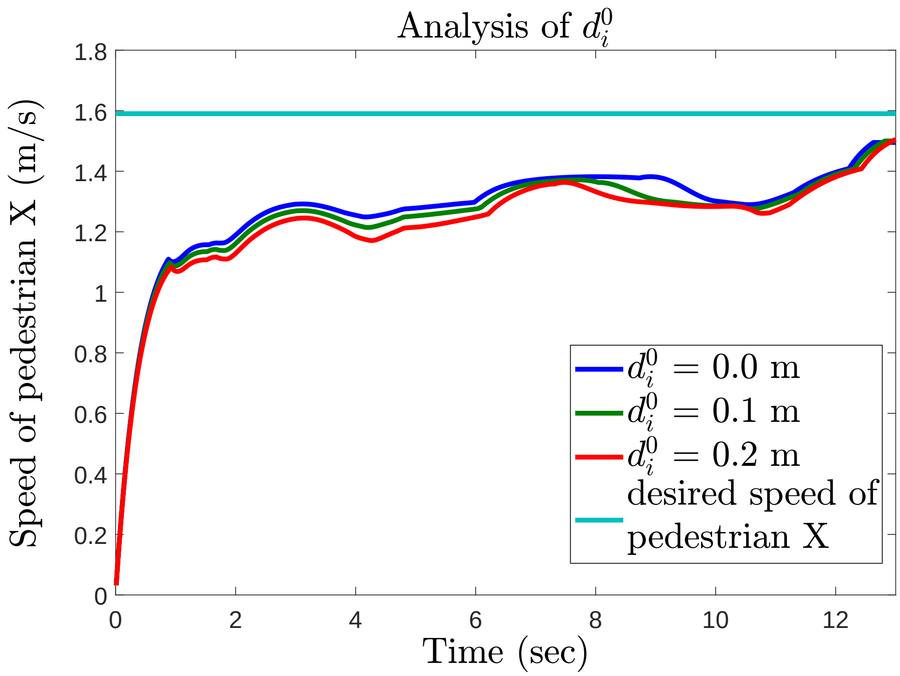

Figure 3.4: Speed of pedestrian X against time for different values of d_i^0.

to τ. In other words, the smaller the value of τ the more strongly the pedestrian is pushed to the target. We also notice that, unlike τ_d, the value of τ does affect the pedestrian dynamics before $t = 1$ s. This is by cause of, as explained earlier, the target force f_i^{tar} being the only force active at the start of the simulation. For the rest of the simulations in this section, we will set $\tau = 0.5$ s, indicating that the pedestrians have a certain hurry in reaching their target. Next, we move on to check the sensitivity of the model parameter d_i^0.

Sensitivity to d_i^0 : In Fig. 3.4 we compare the speed of pedestrian X for three different values of $d_i^0 = 0, 0.1, 0.2$ m. We can see that before $t = 1$ s is reached the values of d_i^0 have no influence on speed. This is because $\boldsymbol{f}_i^{tar}$, the only force initially acting on the pedestrians, is independent of d_i^0. After $t = 1$ s, the effect of changing d_i^0 is similar to the effect of varying τ_d. As d_i^0 gets larger the values of local maxima and

	$r_p = 1$ m	$r_p = 2$ m	$r_p = 3$ m
$r_w = 1$ m	unstable	unstable	unstable
$r_w = 2$ m	unstable	stable	stable
$r_w = 3$ m	unstable	stable	stable

Table 3.1: The stability results for different cutoff radii r_p and r_w values.

minima decrease, while occurring almost at the same time. For values of d_i^0 greater than 0.2 m the system becomes unstable with pedestrian-wall intersections and speed of some pedestrians exceeding their desired speed. From now on, we fix $d_i^0 = 0.2$ m. This may not be a realistic diameter at rest for a person but it is the largest value for which the model reproduces a reasonable pedestrian motion through the corridor.

Sensitivity to the cutoff radii r_p and r_w : The last two model parameters we consider are the cutoff radii r_p and r_w. They provide the largest distance at which a pedestrian and a boundary point could influence the dynamics of a given person respectively. We take all the combinations of values for r_p and r_w reported in Table 3.1. We note that if either of the radii is small the system is unstable. The speed of pedestrians exceed their desired speed in all the unstable cases. Among the stable combinations we consider $r_p = r_w = 2$ m. This combination has less computational cost than the other stable combinations. This is by reason of that the number of pedestrians/wall points needed to compute interaction forces would be greater as the values are higher in the other stable combinations. As a result, we set $r_p = r_w = 2$ m. Finally, we check the numerical convergence of the model with respect to the discretization parameter Δt.

Sensitivity to Δt : Fig. 3.5 displays the speed of pedestrian X for $t \in [0, 13]$

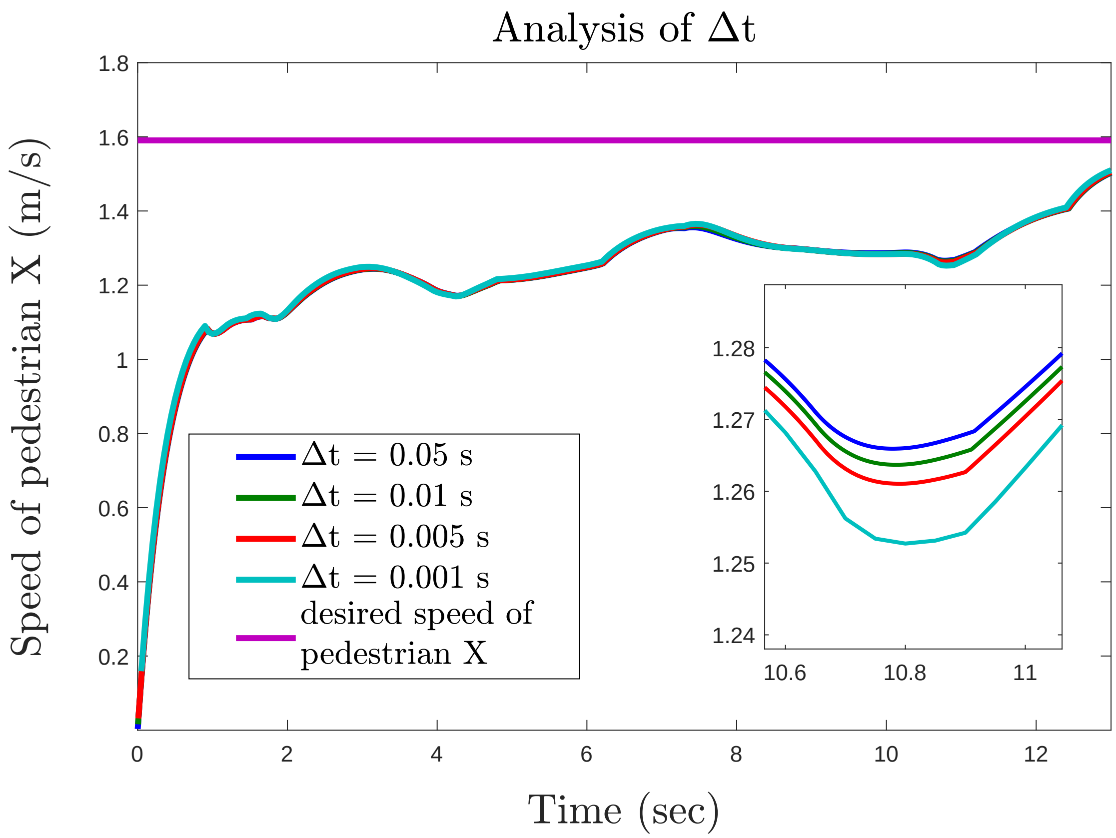

Figure 3.5: Speed of pedestrian X against time for different values of Δt.

s and different values of $\Delta t = 0.05$, 0.01, 0.005 and 0.001 s. We see that for all of these values the dynamics of the pedestrian does not change substantially (within 1%). Thus, we retain $\Delta t = 0.01$ s.

3.3 Overlaps and Oscillations

This section is devoted to the calibration of a key model parameter: the interaction constants in repulsive forces: μ in eq.(2.6) and μ_w in eq.(2.9). We consider $\mu = \mu_w$ for now.

We say an oscillation occurs when a pedestrian's direction deviates more than 90 degrees away from its target direction. An overlap occurs in two scenarios. It could happen when two of the circles representing pedestrians have a non-null intersection, or when a boundary point lies within one such circle. During pedestrian overlaps the effective distance between two people becomes negative.

Let us consider two pedestrians i and j that are close to each other (relative distance d_{ij} is small). In the case where v_{ij} is small as well, the repulsive force in eq.(2.6) with $\mu = 0$ is not sufficient enough to keep the pedestrians far apart to avoid overlaps. The addition of the term $\mu\overline{v}_i$ in the equation thus ensures that there is enough repulsion to avoid overlap. Thus large values of μ help in avoiding overlaps. On the other hand, when v_{ij} is large and d_{ij} is small, a large value of μ may give rise to a strong repulsive force that compels the pedestrian to deviate more than 90 degrees away from the target direction. Thus leading to oscillations. A large value of μ might lead to oscillations in the pedestrian motion and a small value might lead to overlaps. Our goal is to find a value for μ that is large enough to avoid overlaps and small enough to avoid oscillations.

Following [18], we define the overlapping-proportion of a simulation as

$$O_v = \frac{1}{n_{ov}} \sum_{t=0}^{t=T} \sum_{i=1}^{i=N} \sum_{j>i}^{j=N} o_{ij}, \quad \text{with } o_{ij} = \frac{A_{ij}}{\min(A_i, A_j)} \leq 1, \tag{3.1}$$

where o_{ij} quantifies the "overlap-strength"and n_{ov} is the cardinality of the set $\{o_{ij} : o_{ij} \neq 0\}$. A_i and A_j are the areas of the circular discs of pedestrians i and j, and A_{ij} is their area of intersection. If $n_{ov} = 0$, i.e. if no overlap occurs, then O_v is set to 0. Notice that the maximum value that O_v can be is 1.

The oscillation-proportion of a simulation is defined as

$$O_s = \frac{1}{n_{os}} \sum_{t=0}^{t=T} \sum_{i=1}^{i=N} S_i, \quad \text{with } S_i = \frac{1}{2}(-s_i + |s_i|) \quad \text{and } s_i = \frac{v_i \cdot (\overline{v_i}\boldsymbol{e}_i))}{\overline{v_i}^2}, \tag{3.2}$$

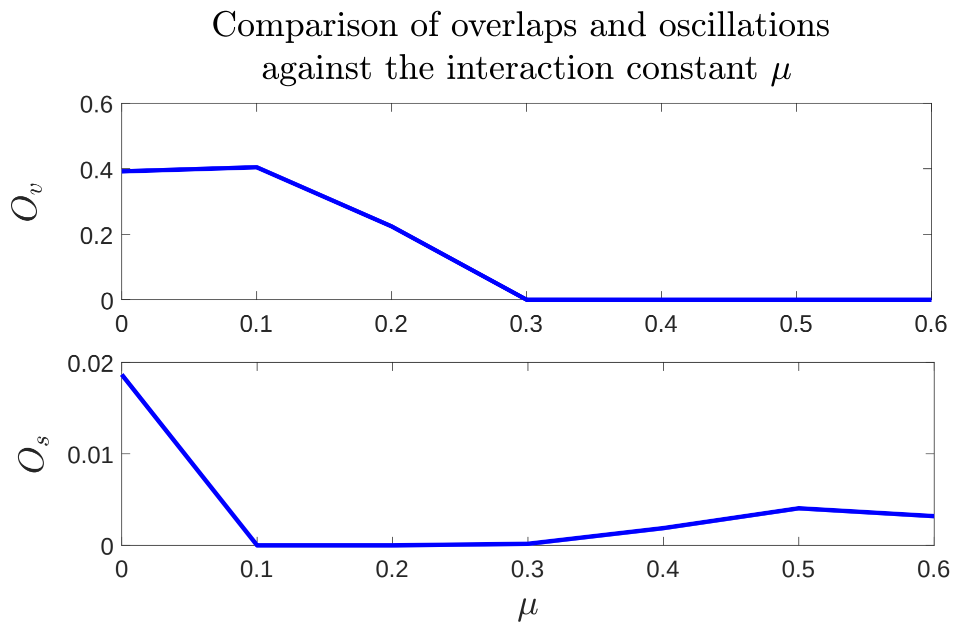

Figure 3.6: Overlap (O_v) and oscillation (O_s) proportions against the interaction constant μ.

where n_{os} is the cardinality of the set $\{S_i : S_i \neq 0\}$. S_i can be viewed as "oscillation-strength" of pedestrian i. If $n_{os} = 0$, i.e. no oscillation occurs, then O_s is set to 0. Similarly to O_v, the maximum value for O_s is 1.

We now set $N = 36$ and retain the values of the other parameters: $\tau = 0.5$ s, $\tau_d = 0.2$ s, $d_i^0 = 0.2$ m , and $r_p = r_w = 2$ m. For different values of $\mu = 0$, 0.1, 0.2, 0.3, 0.4, 0.5, 0.6, we run each set of simulations a 100 times. Fig. 3.6 shows us the average values of O_v and O_s from these 100 runs against μ. Each run uses random desired velocities (Gaussian distributed with mean 1.55 m/s and standard deviation 0.18m/s) for the pedestrians.

From the top plot of Fig. 3.6 we can see that the overlap proportion decreases as μ increases and stays 0 for large values of μ. This is consistent with our earlier analysis that larger the value of μ smaller the overlap. Note that the overlap proportion is a little higher for $\mu = 0.1$ than for $\mu = 0$. This is cause the system became unstable (the speed of some pedestrians exceeded their desired speed). For the same reason we also conclude that oscillation proportion for $\mu = 0$ and 0.1 does not hold any significance. Thus, ignoring these two values, we see from the bottom plot that for small values of μ there is no oscillation. As μ increases, the oscillation proportion increases too, again staying consistent with our earlier analysis that smaller the value of μ smaller the oscillation proportion.

We know that the pedestrians are modeled as circular discs that vary in radius according to the velocity of the pedestrian. Thus we can assume that a pedestrian does not physically occupy the entire disc always. Keeping this in mind, depending on the scenario of an experiment we allow some amount of overlaps in the system, like in the case of $\mu = 0.2$. Choosing $\mu = \mu_w = 0.3$ would be ideal in this experiment yielding no overlaps or oscillations. Choosing $\mu = \mu_w = 0.2$ is also adequate as some overlaps between a large group of people passing through a narrow corridor is acceptable.

Chapter 4

Validation

4.1 Introduction

The process of showing that the numerical method is a good approximation to real life problems is called validation. Validation can be done in a number of ways:

1. Validating using other numerical results.

2. Validating using empirical results.

3. Validating using analytic results.

We validate our model using the aforementioned ways 1 and 2. First, we compare our results against the numerical results obtained with a kinetic theory approach. Next, we compare the macroscopic quantities computed using parameters in our model with empirical ones. Finally, we validate using analytic results that our model can self-organize pedestrians.

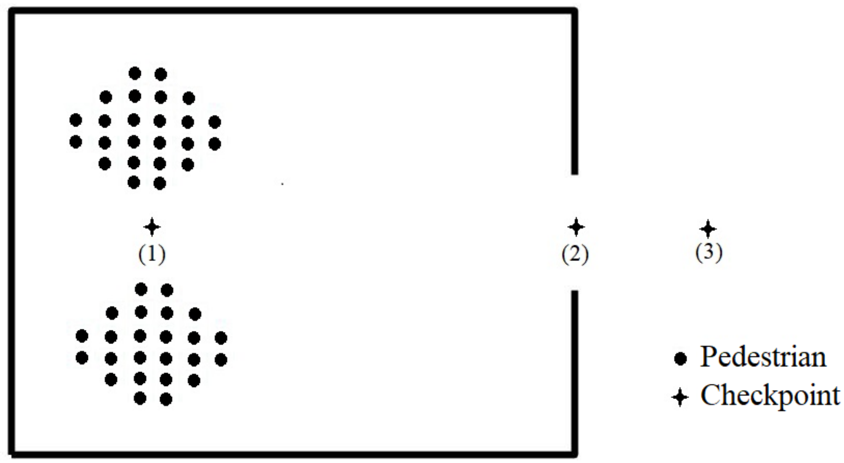

Figure 4.1: A schematic diagram of the square room of length 10 m used as domain where • represents a pedestrian.

4.2 Analysis of Evacuation Time from a Room with Varying Exit Door Size

In this section we consider an experiment from [1] where a kinetic theory approach is presented. The domain for this test is a square room of length 10 m with 48 people inside it, split into two groups as shown in Fig. 4.1. The room has an exit door of width w_{exit} m which is centered at the right wall. The goal of this experiment is to analyze the time taken by these 48 people to exit the room for varying values of w_{exit}. We consider 15 different values of w_{exit} from $[1.2, 4]$ with 0.2 m variation.

In this experiment, we first want the two groups of people to merge into a single group and then walk out of the room. In order to implement this we assign all pedestrians the same path. The path consists of the checkpoints marked 1, 2 and 3 in Fig. 4.1. The radius associated with checkpoint 1 differs for each pedestrian. It varies from $[1, 3]$ m with 0.5 m variation with respect to the initial position of

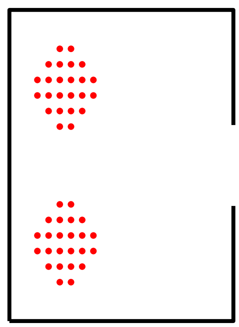

(a) $t = 0$ s

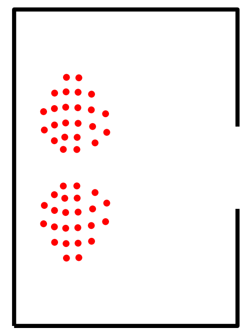

(b) $t = 1.51$ s

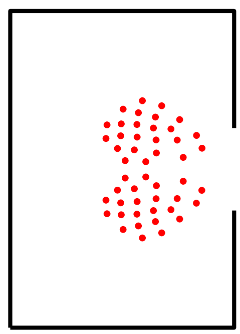

(c) $t = 6.06$ s

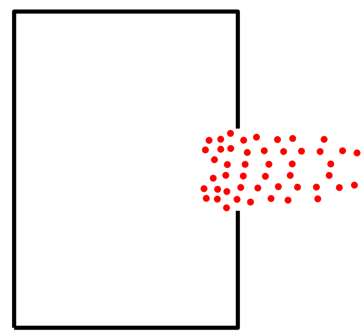

(d) $t = 12.87$ s

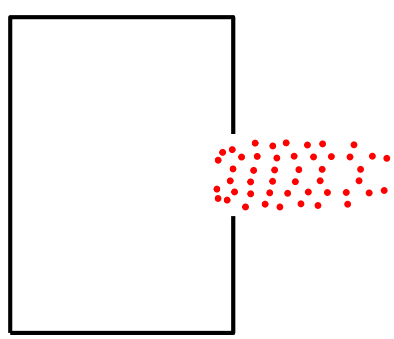

(e) $t = 14.42$ s

Figure 4.2: Screenshots of the pedestrian motion during the evacuation of 46 pedestrians from a square room of length 10 m with exit size $w_{exit} = 2.6$ m at time $t = 0$, 1.51, 6.06, 12.87, 14.42 s.

the pedestrian. The closer a pedestrian is to the checkpoint position, the smaller its radius for checkpoint 1. The radius associated with checkpoints 2 and 3 are set as w_{exit} m and 4 m respectively. We set $dt = 0.01$ s, $\tau = 0.50$ s, $d_i^0 = 0.2$m, $t_d = 0.2$ s, $r_p = r_w = 2$ m. In evacuation scenarios people would tend to move away from walls and would not mind being too close to other pedestrians and thus we set $\mu = 0.20$ and $\mu_w = 0.30$. The desired speed for all pedestrians is set to $1m/s$. Consider the set $\{0.9481, 0.8775, 0.7850, 0.6768\}$ consisting of pedestrians' initial speed values. These values were computed from data in [1]. The initial speed of each person is taken from this set depending upon the density of people around them, i.e the people in the center of the group would have a smaller initial speed than the people at the exterior.

The pedestrian dynamics for the case with $w_{exit} = 2.6$ m is displayed in Fig. 4.2. These plots agree with the results in [1]. At $t = 6.06$s the two groups merge into one with the density of the group high in the interior and low around the edges. As time increases, at $t = 12.87$ s people are crowded near the exit. This flow of motion is consistent with people exiting a room under the conditions of our experiment.

Fig. 4.3 shows us the evacuation time for all cases of varying w_{exit}. We can see that larger the width size of exit door, faster the people exit the room, as one would expect. Note that in the first two cases, even though there is only a small difference in the width of the exit size, the time difference is around 3 s which is high when compared to other values in the plot. This happens due to over crowding near the exit when $w_{exit} = 1.2$ m, implying that this width size is small for a group of 48 people to exit the room smoothly. Also note that for $w_{exit} = 3.4, 3.6, 3.8$ m the evacuation time is constant showing that after a while increasing the width size might not make a difference for the evacuation time.

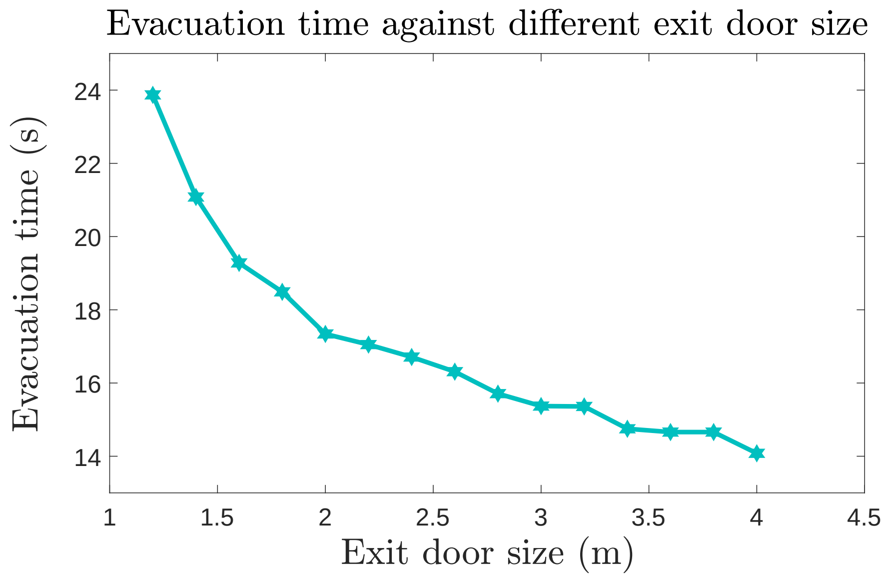

Figure 4.3: Evacuation time of 48 people exiting a square room of length 10 m for varying exit door width.

4.3 Validation Against Experimental Data

In this section we quantitatively validate our model by comparing with the empirical results in [59]. Consider a corridor of length 8 m and uniform width 1.8 m as the space geometry of this experiment (See Fig. 4.4). A perpendicular line passing through this corridor is taken as a reference line. We assign 4 target checkpoints and every pedestrian is assigned the same path : checkpoints 1, 2, 3 and 4. Checkpoint 2 and 4 each have a radius of 1.8 m (width of the corridor), denoted by b_{cor}. Checkpoint 1 has a radius of b_{ent} m and checkpoint 3 has a radius of b_{exit} m, which will vary depending on the experiment. N pedestrians are placed at a distance of 4.5 m away from the beginning of the corridor. The values of b_{ent}, b_{exit}, and N varies for the different experiments. See Table 4.1.

Over a time interval of length δt the macroscopic quantities flux $J_{\delta t}$, average velocity $v_{\delta t}$ and density $\rho_{\delta t}$ are calculated by using the characteristics of people crossing

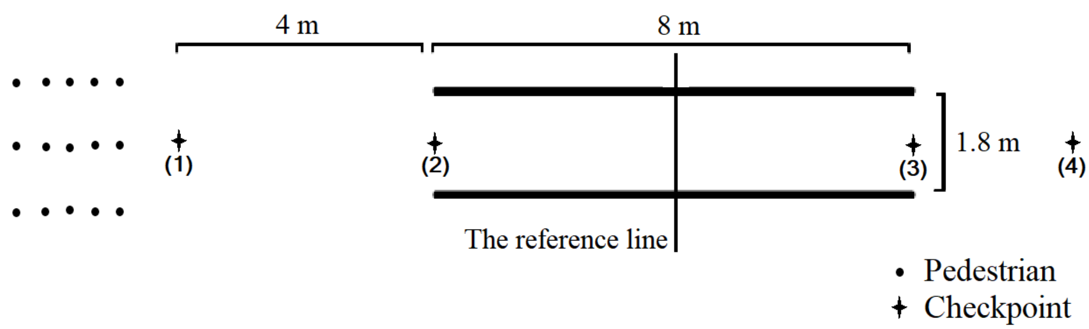

Figure 4.4: A schematic diagram of the corridor used as domain for empirical validation.

the reference line during this time interval. The flux is the rate of flow of pedestrians during the time interval of length δt and hence is computed by:

$$J_{\delta t} = \frac{N_{\delta t}}{t_{N_{\delta t}}}, \tag{4.1}$$

where $N_{\delta t}$ is the total number of people who crossed the reference line during δt and $t_{N_{\delta t}}$ is the time taken by these $N_{\delta t}$ pedestrians to cross the reference line.

The average velocity is given by the equation:

$$v_{\delta t} = \frac{1}{N_{\delta t}} \sum_{i=1}^{i=N_{\delta t}} v_i, \tag{4.2}$$

where v_i is the velocity of the i^{th} pedestrian at the time he/she crossed the reference line.

Finally the density is computed as:

$$\rho_{\delta t} = \frac{J_{\delta t}}{v_{\delta t} b_{cor}}. \tag{4.3}$$

For every experiment we will compare the computed and measured macroscopic quantities. Following [59] we set the reference line to be 4 m from the start of the corridor, i.e the reference line splits the corridor into two and also set $\delta t = 10$ s.

Experiment Index	N	b_{ent} $[m]$	b_{exit} $[m]$
1	60	0.50	1.80
2	66	0.60	1.80
3	111	0.70	1.80
4	121	1.00	1.80
5	175	1.45	1.80
6	220	1.80	1.80
7	170	1.80	1.20
8	160	1.80	0.95
9	148	1.80	0.70

Table 4.1: The 9 different experiment values considered for empirical validation.

For every experiment we need to decide when the time interval of δt seconds starts during the simulation. From Fig. 4.4 we can see the initial positioning of the pedestrians. If we consider $[0, \delta t]$ s as the interval of consideration for computing the quantities for every experiment, then varying N would not make much of a difference. Also for small values of b_{ent}, the time interval under consideration might have passed even before the pedestrians reach the reference line. Thus we set the interval of consideration to be $[start, start + \delta t]$, where the value of start changes for the different experiments in Table 4.1. To explain how we pick the value of start, we consider experiment 1, which features $N = 60$, $b_{ent} = 0.50$ m and $b_{exit} = 1.80$ m. Fig. 4.5 shows the computed density against average velocity for different start times. We see that when the time interval starts during the first $10 - 30$ s of the simulation, the density values are close to each other and thus we set the start time of this

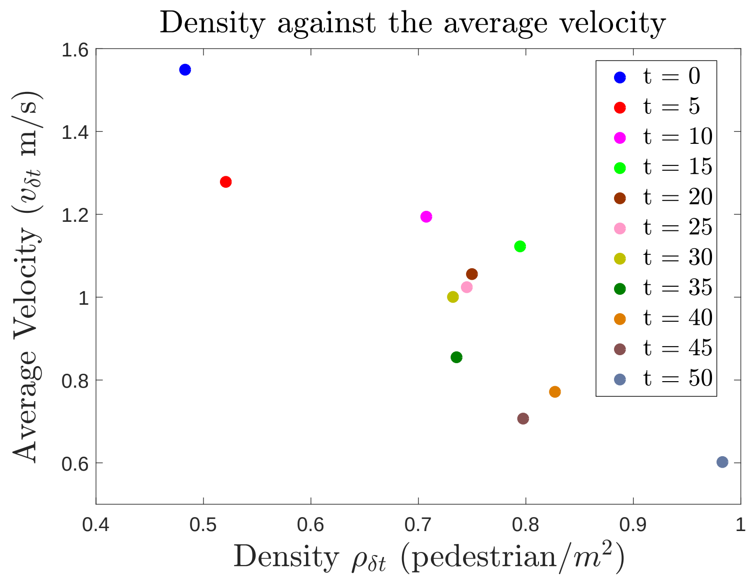

Figure 4.5: Density against average velocity for different start times with 50 pedestrians, $b_{ent} = 0.5$ m, and $b_{exit} = 1.8$ m

experiment to be 10 s after the beginning of simulation. The start time for each of the experiments are set in a similar manner. Once the start times are decided, the densities and average velocities during the interval of consideration are computed for a total of 6 runs.

Fig. 4.6 shows the fundamental diagram of the density plotted against the average velocity for each experiment in Table 4.1 using two different approaches. We can observe from this figure that the results we obtained are in good agreement with the empirical data in [59]. Consider experiments 1 through 6. These experiments differ by the increasing values of both N and b_{ent}, with constant b_{exit}. For these cases the computed density increases too. This is expected as the larger the population, the higher the density. Due to the fixed corridor width, as the population increases, the speed of people decrease to allocate other pedestrians. Thus resulting in lower average velocities. Now, consider the experiments 6 through 9. In this set, b_{ent} is

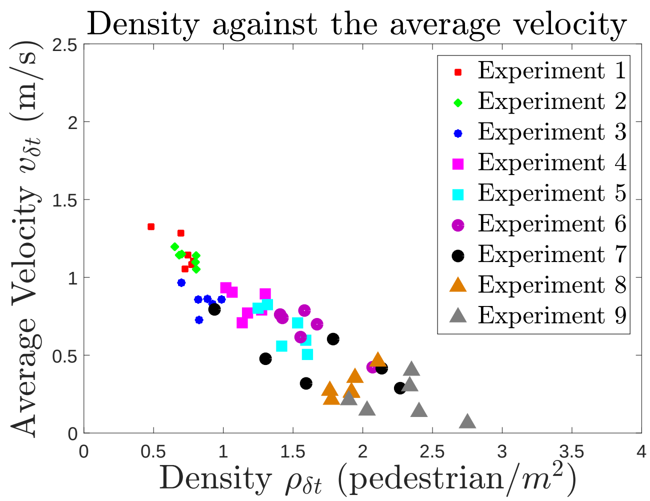

(a) Experimental results from our model

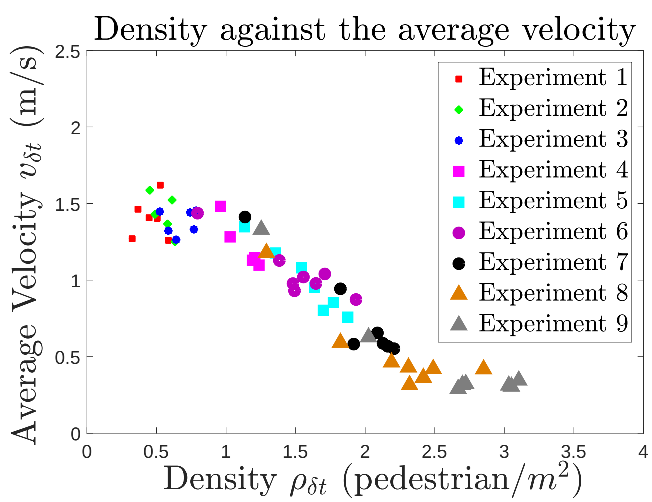

(b) Empirical results from [59]

Figure 4.6: The fundamental plots of density against average velocity for all the 9 experimental data values in Table. 4.1 using two different approaches.

constant with decreasing N and b_{exit}. These cases yield higher density values too. As the length of b_{ent} is wide enough, even with a decrease in population, the density grows higher. As b_{exit} value reduces, people trying to exit the corridor cluster near the exit. Consequently, the people at their back slow down. Thus, more people cross the reference line with low velocities, inducing high densities.

In the above validation process, we validated our calibrated model with empirical results. The important thing to note here is that our model parameters were tuned only using a sample experiment with the same domain as the empirical experimental setup. Considering that they were not tuned to specifically match the empirical results, the consistent behavior of our model and the empirical results is a strong indication that our model simulates pedestrian motion well.

4.4 Lane formation

So far the experiments had a unidirectional flow of pedestrians. In this section, we see how the model works when we consider a bidirectional flow. In real life, when groups of people approach each other from opposite directions, they form lanes naturally making the pedestrian movement undisrupted (see [31, 29, 58]). A good people dynamics model has to accommodate such natural behavior and so we test our model against this scenario.

We split the pedestrians into two equal groups and place them in a corridor of length 20 m and width 5 m (see Fig. 4.7). Group 1 has the objective of moving to the right exit (target checkpoint for Group 1 with radius 5 m) and Group 2 has to move towards the left exit (target checkpoint for Group 2 with radius 5 m). Once they exit we reintroduce the pedestrians into the corridor from the opposite exit to mimic

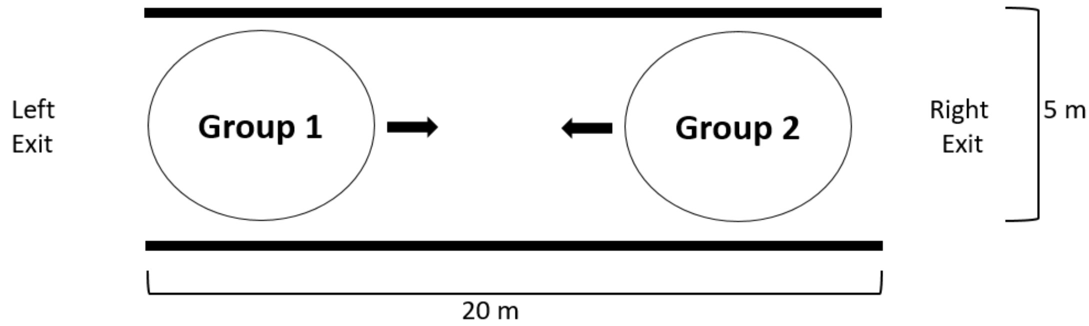

Figure 4.7: A schematic diagram of the corridor used as domain in lane formation experiments.

periodic boundary conditions. We vary the density of pedestrians inside the corridor ρ from 0.2 to 1.6 $pedestrians/m^2$ with change in density $\Delta\rho = 0.2$ $pedestrians/m^2$. The number of pedestrians for each experiment is thus calculated by

$$N = \rho * A(C) \tag{4.4}$$

with $A(C) = 100\ m^2$ denoting the area of corridor. Higher values of ρ were not considered as they led to an unstable system. We take $dt = 0.01$ s, $\tau = 0.50$ s, $d_i^0 = 0.2$m, $t_d = 0.2$ s, $r_p = r_w = 2$ m, $\mu = 0.20$ and $\mu_w = 0.20$ for all the cases in this section. All pedestrians have a desired goal velocity of 1 m/s.

We note that when the simulation starts the pedestrians reduce their speed due to their interaction with the opposite stream of pedestrians. In fact, the pedestrian repulsive force f_{ij}^{ped} is large as the relative velocity component v_{ij} among them will be high (as the velocities are in opposite directions). This behavior is observed for all pedestrians interacting with pedestrians of opposite stream. We also note that the row of pedestrians near the wall tend to move closer to the wall when they encounter the opposing stream of pedestrians. This is by reason of the repulsive force from pedestrians f_{ij}^{ped} being higher than that of the wall f_{ij}^{wal}. The initial positioning of the

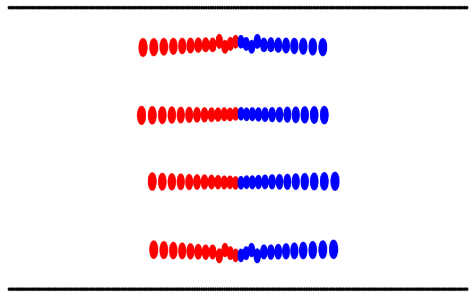

Figure 4.8: The frozen state of 100 pedestrians induced by initially positioning two groups of people as mirror images of each other.

Density (ρ)	0.2	0.4	0.6	0.8	1.0	1.2	1.4	1.6
Number of pedestrians (N)	20	40	60	80	100	120	140	160
Number of lanes	2	2	2	2	2	2	4	4

Table 4.2: The number of lanes formed in each of the 8 experiments that vary by density ρ and hence by number of pedestrians N.

pedestrians is such that once the simulation starts and they get close to the opposing stream they have some space between them to move away from each other. If the initial positioning of pedestrians were mirror images then, we end up with a $frozen$ state (see Fig. 4.8) where all the pedestrians collide head on and stop before producing an unstable system.

Table. 4.2 reports the number of lanes formed in each of the experiments considered. We observe that as density ρ increases, the number of lanes eventually increase too. This is displayed in Fig. 4.9 for the cases with density $\rho = 1$ and 1.4 $pedestrians/m^2$. Note that the initial interaction forces in the simulations are symmetric as the initial positioning of the pedestrians in the two groups are symmetric

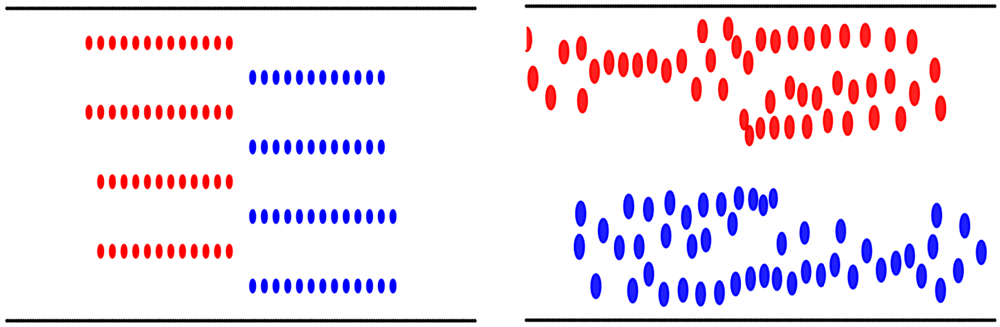

(a) The 2− lane formation induced by 100 pedestrians

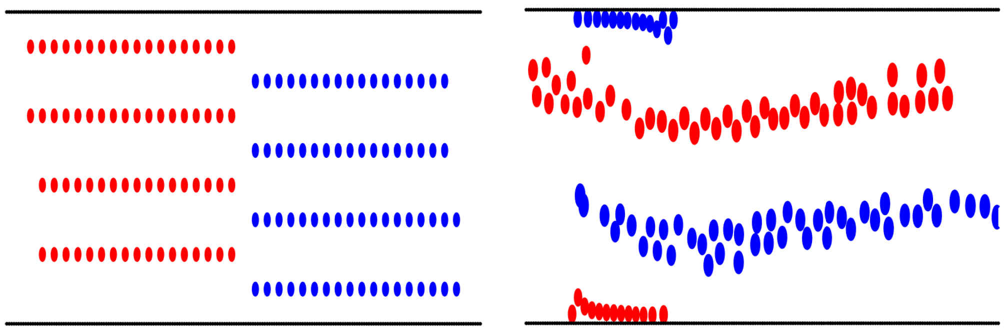

(b) The 4− lane formation induced by 140 pedestrians

Figure 4.9: On the left we have the initial positioning of the pedestrians and on the right we have the final lane formation.

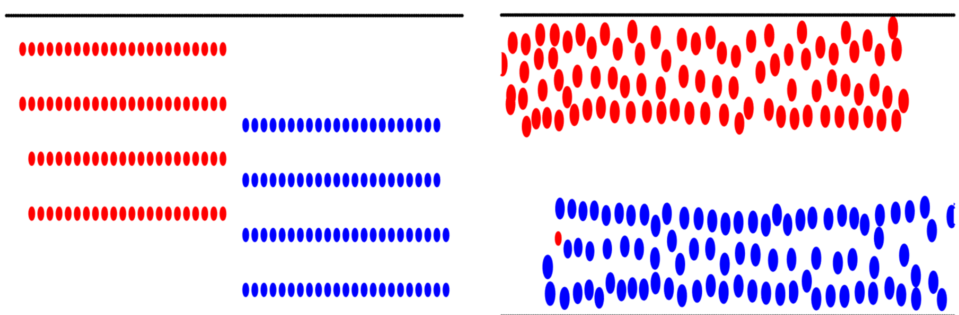

Figure 4.10: On the left we have the initial positioning (different from the cases listed on Table 4.2) of 180 pedestrians and on the right we have the final 2-lane formation.

(left plots in Fig. 4.9). The target forces are also symmetric due to the boundary conditions. This leads to a symmetric lane formation (right plots in Fig. 4.9).

When we considered the case of 180 pedestrians ($\rho = 1.8\ pedestrians/m^2$), we could not simulate a stable system for this set of initial positions. This is an indication that this model does not handle high densities well. However, when the initial positioning was changed (see Fig. 4.10), we end up with a $2-$ lane and not a $4-$ lane formation even though the density was high. This suggests that the number of lanes is influenced not only by the crowd size but also by the initial positioning. When the densities were increased further, even a change in initial positioning could not help in achieving a stable system. This further reinforces the fact that the model does not perform well for high densities.

In Chapter 3, we calibrated the model proposed in Chapter 2 to obtain values for model parameters. Here, we used these tuned parameter values in the model to simulate various experiments, in order to validate it against numerical and empirical results. This has shown that our model works well for simple domains, where the pedestrians have straightforward paths. We now extend our model by introducing 'contact tracking' to trace an infectious disease. We then apply our model to more complex domains, assigning complex paths to the pedestrians.

Chapter 5

Contact Tracking Model and Numerical Simulations for Airborne Disease Spreading

5.1 Introduction

Contact tracing is a method for identifying all the people who could have been infected by a disease as a result of direct contact with a sick person. A sick person who could potentially infect other people with their disease/infection is termed as a *primary contact*. A person is termed a *secondary contact* if they got infected by a primary contact due to sufficient contact between them. Once the secondary contacts are aware of their exposure to the disease, necessary measures could be taken to diagnose them and later treat them if needed. Depending on the nature of the disease, sufficient contact is influenced by factors like place, duration of contact and the vulnerability of the healthy person. The main purpose of contact tracing is to detect the early symptoms of the disease on secondary contacts, observe and treat them if possible. This process is meant to stop infections and diseases spreading further through the community and hopefully prevent an outbreak of the disease.

To quantify the transmission dynamics from a sick individual to a healthy one, the basic reproduction number R_0 has been used to measure the average number of secondary contacts generated. Most models predicting the severity of an epidemic and the basic reproduction number are based on the averaged large population [14, 39, 35]. Such models typically do not work on scenarios when the number of infected individuals is small and the size of healthy population is medium, as in the case of airports and hospital emergency rooms. Contact tracing associated with such environments is of paramount importance for an early suppression of an epidemic.

Our main focus is to track the transmission of an infectious disease in an airport involving medium size populations consisting of both susceptible and non-susceptible healthy individuals, and a small number of infectious individuals. The average number of secondary contacts, denoted by Avg_{sc}, for various percentage of susceptible individuals in the system are analyzed.

5.2 Mathematical Model

Let us consider a group of N pedestrians in a geometry Ω. The pedestrian dynamics are modeled as in Chapter 2 over a time interval of interest $(0, T]$. Pedestrians have a characteristic to be one among the following - infectious (sick), non-susceptible (immune), susceptible (vulnerable), infected and not infected. These characteristics are known as *stages*. Consider the following sets consisting of the indices of pedestrians:

$$\mathcal{S} = \{i \in \mathbb{N}, i \leq N \ : \ i^{th} \ pedestrian \ is \ susceptible/vulnerable\},$$

$$\mathcal{I} = \{i \in \mathbb{N}, i \leq N \ : \ i^{th} \ pedestrian \ is \ infectious/sick\},$$

where $\mathcal{S}$ denotes the set of all pedestrians that are vulnerable to being infected by sick people and $\mathcal{I}$ is the set of all pedestrians that are infectious/sick (people who can transmit the disease).

Initially, among the N pedestrians, we take P_{imm} % of the pedestrian population to be immune (people who cannot be affected by sick people) and a small number of people to be sick. Rest of the population would consist of people vulnerable to the disease. Thus, in the beginning, every pedestrian is categorized into one of these stages: sick, immune and vulnerable.

For an sick person i with position $\boldsymbol{r}_i$, we define the set of all susceptible pedestrians that lie inside its circle of influence (sickness domain) at a certain time $t \in (0, T]$ as:

$$\mathcal{I}_i^{sus} = \{j \in \mathcal{S} \ : \ ||\boldsymbol{r}_j - \boldsymbol{r}_i|| \leq r_s\}, \ i \in \mathcal{I},$$

where $\|.\|$ denotes the Euclidean norm in $\mathbb{R}^2$, and r_s is the cutoff radius for the circle of influence. If a pedestrian $j \in \mathcal{I}_i^{sus}$ for a continuous period of time, e.g. t_{vul} minutes, then they have a v_s % probability of getting infected. Furthermore, j would no longer belong to $\mathcal{S}$ and would be moved to either one of the following sets according to its updated stage:

$$\mathcal{E}_{sick} = \{j \in \mathbb{N}, \ : \ j \in \mathcal{I}_i^{sus} \ for \ t_{vul} \ mins \ and \ is \ infected\},$$

$$\mathcal{E}_{safe} = \{j \in \mathbb{N}, \ : \ j \in \mathcal{I}_i^{sus} \ for \ t_{vul} \ mins \ and \ is \ not \ infected\}.$$

$\mathcal{E}_{sick}$ denotes the set of all pedestrians who have been exposed to the disease for t_{vul} minutes and have fallen sick. $\mathcal{E}_{safe}$ denotes the set of all pedestrians who have been exposed to the disease for t_{vul} minutes but were not affected. Once a vulnerable pedestrian moves to either of these sets, they would no longer be considered as an element of $\mathcal{S}$, i.e.,

$$\mathcal{S} \cap \ \mathcal{E}_{sick} = \mathcal{S} \cap \ \mathcal{E}_{safe} = \emptyset.$$

In other words, once a pedestrian belongs to either one of the sets $\mathcal{E}_{sick}$ or $\mathcal{E}_{safe}$, they are no longer considered to be in the pedestrian population that could get infected by sick people. We also assume that pedestrians who belong to $\mathcal{E}_{sick}$, though infected, will not be able to further transmit the disease.

5.3 Numerical Simulations

5.3.1 Introduction

In this chapter we consider a case where sick people enter an airport via the entrance and board a plane. Then, they land at a different airport, deplane and enter via the terminals into the airport and board another plane. The disease spread is not tracked during the course of flight. By varying N, P_{imm} and the number of primary contacts, a series of simulations are run to calculate Avg_{sc}.

Consider the domain Ω to be a small portion of Houston's William P. Hobby Airport. The dimensions were obtained from Google Maps, See Fig. 5.1. Initially, there are N pedestrians in the system. Each pedestrian is randomly categorized at the start to be either sick, immune or vulnerable. The incoming flow of pedestrians is either through the airport *entry* or through the *terminals* from deplaning. The outgoing flow is either through the airport *exit* or through the terminals for boarding the plane.

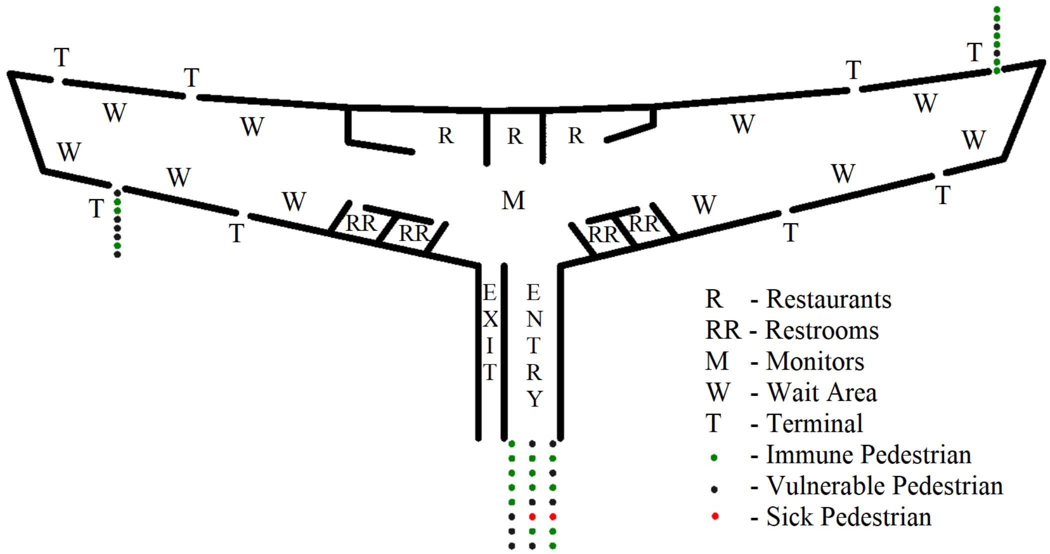

Figure 5.1: A portion of the William P. Hobby Airport in Houston, TX. Pedestrians are represented with a •. The group of pedestrians is small for representation purposes.

Pedestrians are assigned a random path to pass through the airport. Some people deplane, enter the airport through the terminal gate and leave the airport via the *exit* corridor with the option to stop by restrooms or restaurants. Others enter the airport through the *entry* corridor and walk to their alloted terminal gate with options to use the restrooms or restaurants before they board their plane. People are also assigned to randomly check out display monitors for their departure times in their path. Appropriate wait times are allocated for each checkpoint that denotes a restroom, restaurant or a display monitor. This is done to make sure that people spend the respective *wait time* at these checkpoints. Finally, if a person reaches the gate before their plane's boarding time, they move on to one of the *wait areas* (see. Fig. 5.1) near their assigned terminal gate until it is time to board.

In Chapter 2, each pedestrian was assigned checkpoints from a list of checkpoint positions according to their path. As the domain in this case has more complicated shape than the previous domains used, each pedestrian's checkpoint assignment is now chosen in a different way. The list of checkpoints contains a checkpoint i's position and a radius r_i associated with it. If checkpoint i is in the path of a person, the position of that person's checkpoint is randomly picked to be a point inside a circle of radius r_i centered at checkpoint i's position. This makes each pedestrian's checkpoints unique (if truly random). Assigning checkpoints this way helps to avoid oscillations in pedestrian motion while pedestrians are cluttered around checkpoints that have wait times. Such an assignment also helps in well distributed pedestrian positioning inside domain Ω.

Code Implementation: The simulations are implemented as C++ applications in Microsoft Visual Studio. OpenGL was used to visualize the pedestrian motion and observe the spread of disease with time. The simulations are run on a shared 40-core computing server with 512 GB RAM. Each simulation starts by initializing the pedestrian positions, velocities, stages and paths. At each time step, the new position of all the pedestrians are computed based on the forces acting on them. The pedestrian velocity is then updated using this new position. Further, newly infected pedestrians are also identified at each time step.

5.3.2 Departing from an Airport

The first airport under consideration is part of the William P. Hobby Airport in Houston,TX - see Fig. 5.1. As the airport has 8 terminals, people who enter via the entry , have the option to board planes through 8 different terminals. We assign only 2 groups of people to deplane and leave the airport. People who deplane only start doing so when it is their time to arrive into the airport. Similarly, people who board planes only do so when it is their time to depart.

The microscopic dynamics model parameters are set as follows: $dt = 0.01$ s, $\tau = 0.5$ s, $\tau_d = 0.18$ s, $r_p = r_w = 2$ m, $d_i^0 = 0.20$ m, and $\mu = \mu_w = 0.3$. The contact tracking model parameters are set as follows: The cut-off radius $r_s = 2.5$ m and the probability of getting infected, if vulnerable, $v_s = 90\%$. The latter is a realistic value for a highly infective disease like, e.g., measles.

Each of the cases that follow vary the values of $P_{imm} = 90\%$, 85%, 80%, 75%, 70%, 65%, 60%, 55% for each of their run. For each P_{imm}, 200 simulations are run to calculate the average number of secondary contacts yielded denoted by Avg_{sc}.

We will consider two cases: a simple case to test our code (case 1) and a more realistic case (case 2).

Case 1: Set the number of pedestrians $N = 400$, the total time of the simulation $T = 15$ minutes and the amount of time to potentially get infected $t_v = 1$ minute.

a) Set the number of primary contacts to be 1.

b) Set the number of primary contacts to be 2.

Case 2: Set the number of pedestrians $N = 1000$, the total time of the simulation $T = 60$ minutes and the amount of time to potentially get infected $t_v = 2$ minutes.

a) Set the number of primary contacts to be 1.

b) Set the number of primary contacts to be 2.

Note that in Chapter 4, we concluded that our model does not perform very well with high density of pedestrians. The two cases we have considered above are of low densities (both with respect to the whole airport domain and with wait areas inside the airport). As per expectation, we observed that our model could handle these efficiently.

Figure 5.2: Screenshot of the airport 5 minutes into the start of the simulation. Pedestrians are represented with a • and each color represents the different stages (immune, vulnerable, and sick).

Let us now see how a typical simulation looks like. Fig. 5.2 represents the airport 5 minutes into the start of a simulation. Red dots denote primary contacts, black dots represent vulnerable people and green ones denote people immune to the disease. Notice that the primary contact enters the airport via the entry and is yet to have any effect on its surrounding people. This is not surprising since we are early into the simulation. Some people are at restaurants, some are inside the restrooms, some are on the way to their next checkpoint and some are in their allocated wait areas ready to board. We also see that people are deplaning from the terminal on the right. This figure gives us a good representation of what happens inside the airport early in the simulation.

Fig. 5.3 shows us how the airport might look like at the end of a simulation. Note that we have 2 different colored dots added to this system, and the number

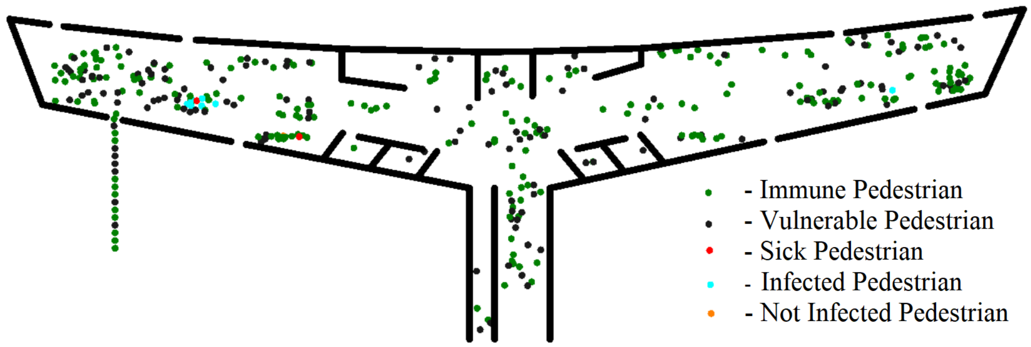

Figure 5.3: Screenshot of the airport after the spread of disease occurs. Pedestrians are represented with • and each color represents the different stages (immune, vulnerable, sick, infected and not infected).

of primaries now set to 2. Blue dots denote secondary contacts or infected people. Orange dots represent people were affected by the primary contact but not infected. Observe from Fig. 5.3 that a group of people turned blue around a primary contact on the left in the wait area. This is a strong indicator that wait areas are a common place to get infected. Also, there is a secondary contact on the right of the airport with no primary in its vicinity. Given the current positions of the primaries (left), and the current position of the secondary (right), it is evident that they could have crossed paths in the corridor or in a restroom/restaurant of the airport, and not in a wait area. This shows us that a secondary contact does not necessarily have to catch the same plane as a primary.

Now that we have a good visual idea of how the simulations run, we move on to the analysis of results from case 1 and 2. Fig. 5.4 shows the average number of secondary contacts for varying P_{imm}. We note that except for the outlier at $P_{imm} = 75\%$ for case 1, the curves of each case have a steady increase in slope. A trivial observation is that for same population size, an increase in primaries causes an increase in Avg_{sc}

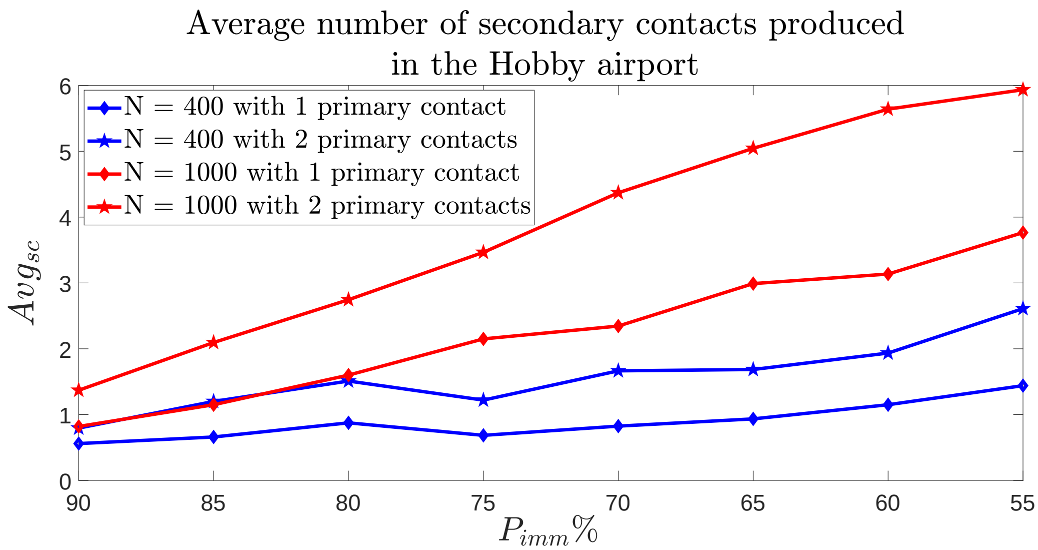

Figure 5.4: Average number of secondary contacts produced inside Hobby Airport for varying immune percentage of pedestrians.

for the sub cases in Case 1 and 2. We also note that the difference between Avg_{sc} of cases in 1 increases very slowly with P_{imm} decrease. In case 2, the difference between Avg_{sc} increases faster than in case 1, implying that the larger the value of N, the higher the rate of increase of Avg_{sc}.

In Fig. 5.5 we compare the frequency distributions of case 1(a) (top plot) and case 2(b)(bottom plot). These cases were chosen to compare the extreme scenarios. Clearly, both the distributions are skewed. From the top plot we note that the mode of every distribution is 0 but the mode of the bottom plot is non zero for all distributions. We also note that the top plot is a concave curve and that the bottom one is a convex one. This means that when N increases, the chances of the number of secondary contacts being small decreases.

In Tables 5.1 and 5.2, we can see that with decrease in P_{imm}, the standard deviation of the number of secondary contacts also increases. This indicates a wider range of values for the number of secondary contacts with decrease in P_{imm}. This

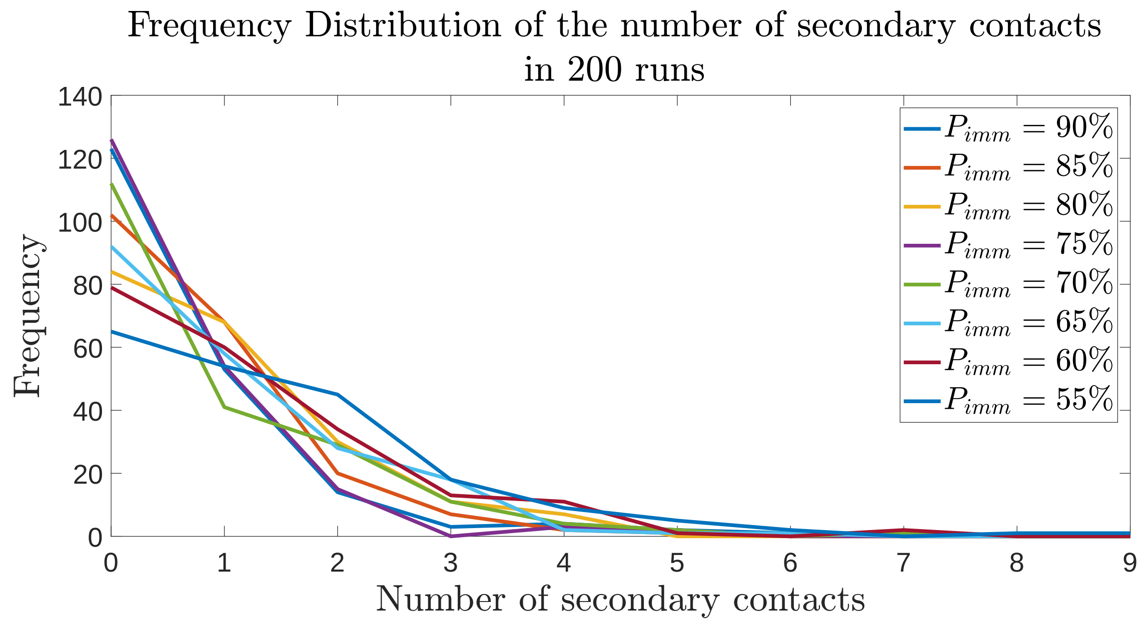

(a) $N = 400$ with 1 primary contact.

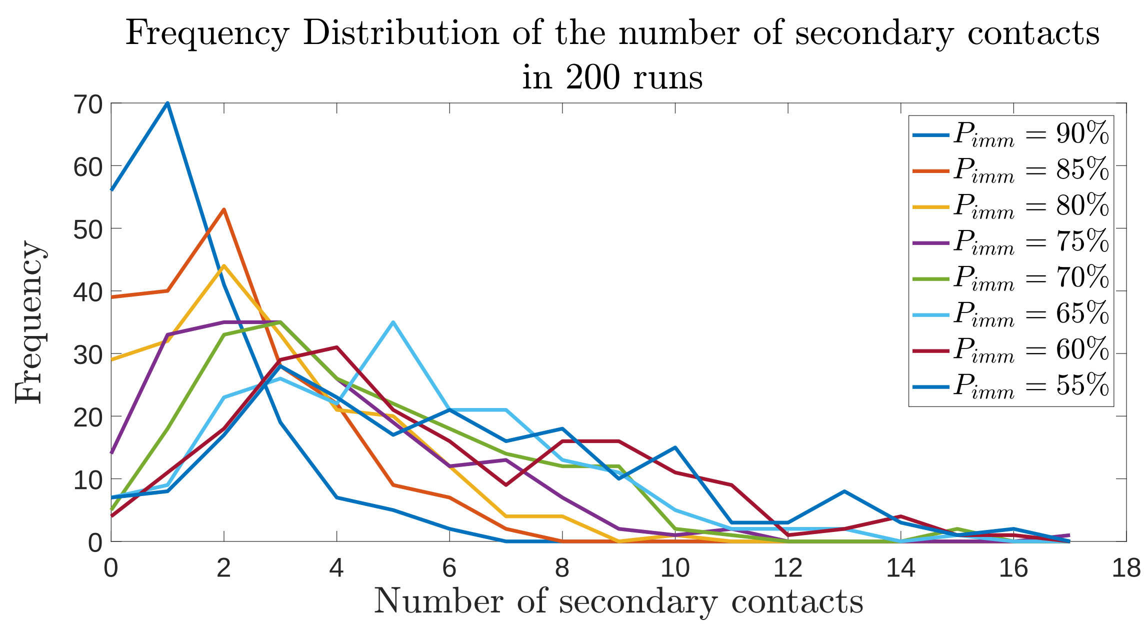

(b) $N = 1000$ with 2 primary contacts.

Figure 5.5: Frequency distribution of the number of secondary contacts produced in 200 runs inside the Hobby Airport, for varying P_{imm}.

$P_{imm}\%$	90	85	80	75	70	65	60	55
Avg_{sc}	0.56	0.66	0.88	0.69	0.83	0.94	1.15	1.44
Sd_{sc}	0.93	0.85	0.99	1.19	1.19	1.12	1.31	1.53
Max_{sc}	4	4	4	7	7	6	7	9

Table 5.1: The computed average number of secondary contacts Avg_{sc}, standard deviation for all 200 runs (Sd_{sc}) and maximum number of secondary contacts in an experiment among all the runs (Max_{sc}) for $N = 400$ and 1 primary contact in the airport.

is also reinforced by Fig. 5.5, where the curves for larger P_{imm} values have taller, narrower peaks as opposed to the curves with smaller P_{imm} values, which have shorter, broader peaks.

Taking a bus to board the flight

An infectious disease in general has a higher chance of spreading if the sick person is in a crowded place. Bearing this in mind we extend our previous airport geometry to include the transportation buses that pedestrians board before they get on their flights. Every pedestrian who departs from the airport will now have their final checkpoint as a random position inside a bus. The checkpoint corresponding to a bus has a wait time of 5 minutes, i.e., once a plane's passengers are all inside the bus they stay inside it for 5 minutes and then are assumed to board the plane, thus leaving the simulation. Fig. 5.6 is a screenshot of how the airport with buses typically looks like, once people have boarded the bus. The dimensions 5x12 m^2 of the bus are chosen in order to accommodate 50 pedestrians in it.

$P_{immune}\%$	90	85	80	75	70	65	60	55
Avg_{sc}	1.37	2.10	2.75	3.47	4.37	5.05	5.64	5.94
Sd_{sc}	1.30	1.66	2.04	2.53	2.69	2.80	3.37	3.57
Max_{sc}	6	7	10	17	15	15	16	16

Table 5.2: The computed average number of secondary contacts Avg_{sc}, standard deviation for all 200 runs (Sd_{sc}) and maximum number of secondary contacts in an experiment among all the runs (Max_{sc}) for $N = 1000$ and 2 primary contacts in the airport.

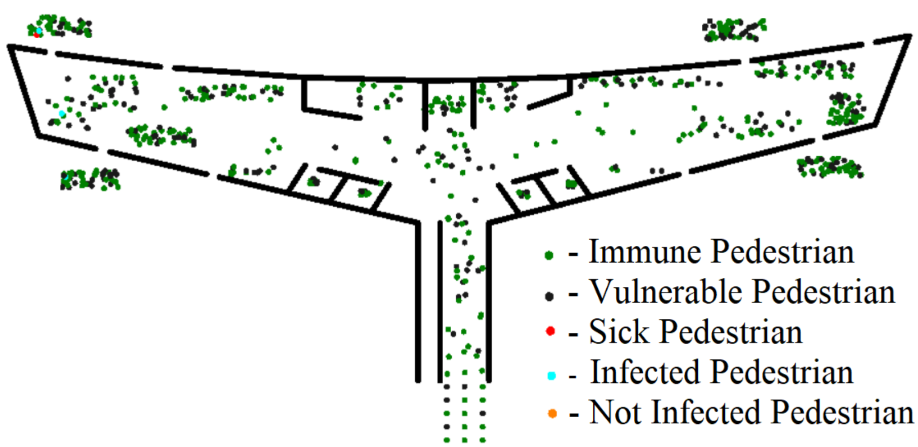

Figure 5.6: Screenshot of the Hobby airport after some pedestrians have boarded their buses. Pedestrians are represented with a • and each color represents the different stages (immune, vulnerable, sick, infected and not infected).

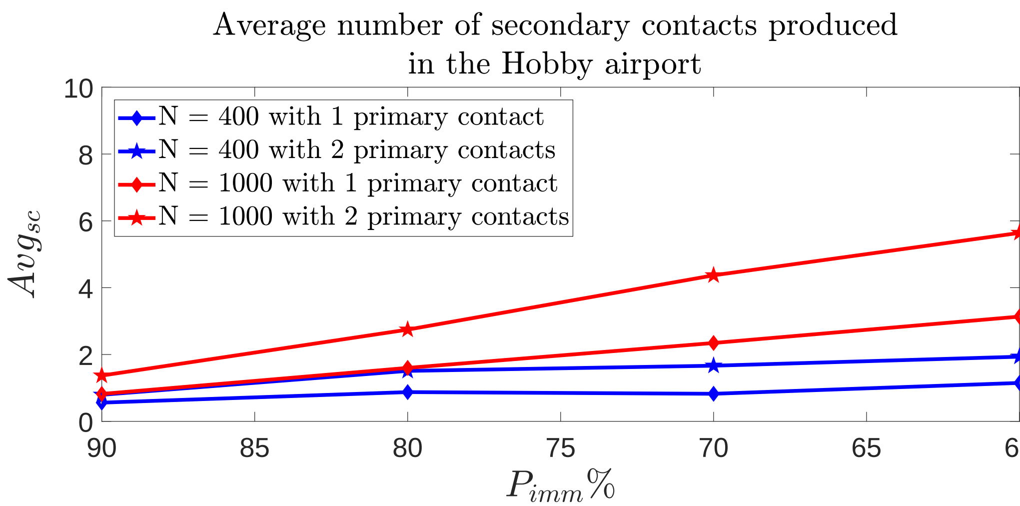

(a) Without buses.

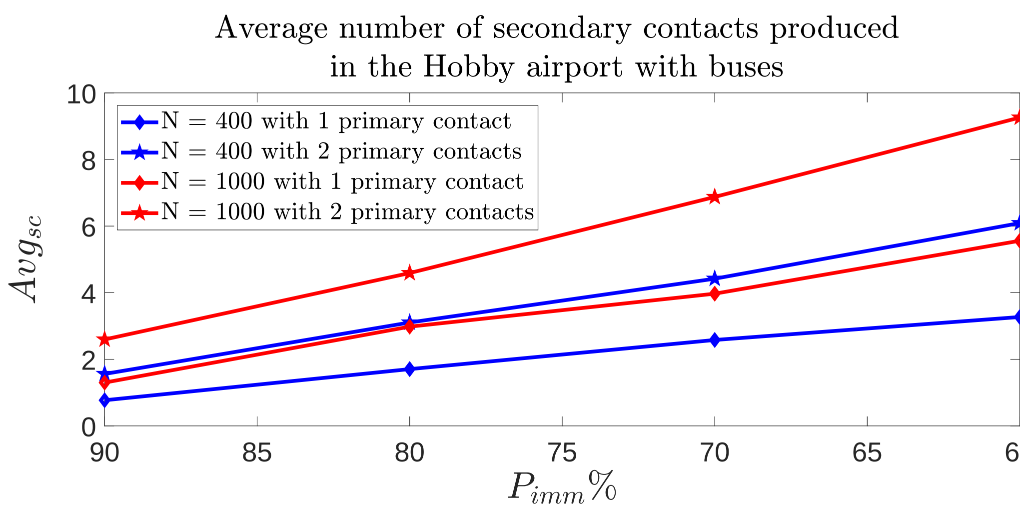

(b) With buses.

Figure 5.7: Average number of secondary contacts produced in 200 runs for varying immune percentage of pedestrians.

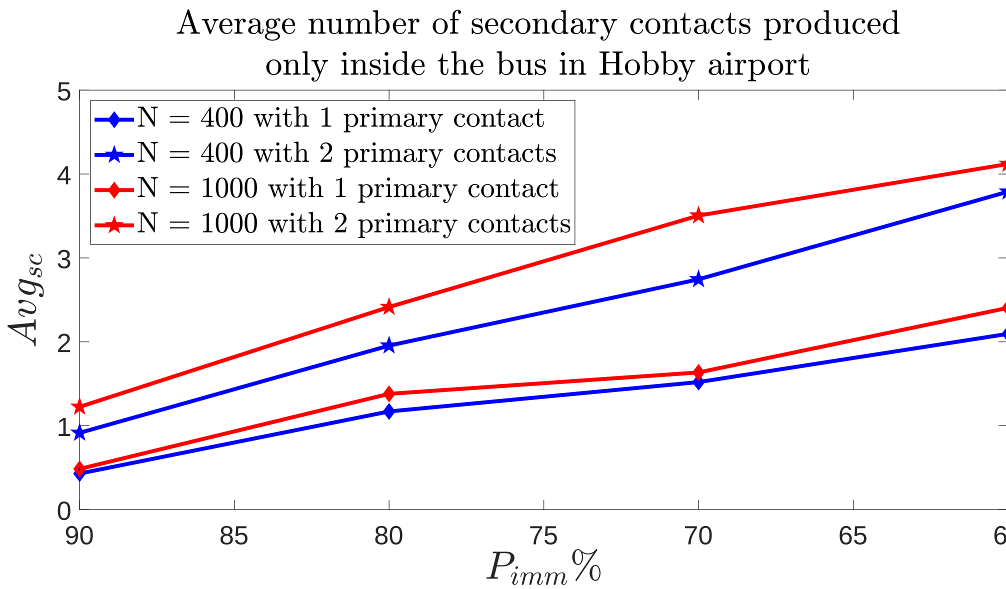

Figure 5.8: Average number of secondary contacts for 200 runs produced only inside the bus in Hobby airport for varying immune percentage of pedestrians.

We repeat all our previous cases in Sec. 5.3.2 to calculate Avg_{sc} for $P_{imm} = 90\%$, 80%, 70%, 60%. Fig. 5.7 shows the averages of these cases along with the ones with no buses. From the right plot in Fig. 5.7, we see that the increase in primaries increases Avg_{sc}. Also, the larger the value of N, the higher the rate of increase of Avg_{sc} when P_{imm} decreases. These observations are consistent with the findings in the left plot with no buses, which were already analyzed in Sec. 5.3.2. Note that having a high density area such as a bus in the path of pedestrians drastically increases the rate at which people could potentially get infected. This is observed in the bottom plot in the case with $N = 400$ with 2 primaries where its Avg_{sc} values end up having higher values than that of the case with $N = 1000$ with 1 primary.

Fig. 5.8 shows us the average number of secondary contacts infected inside the bus. We can see that the cases with the same number of primaries have average values closer to each other. This is due to the fact that even though the difference between

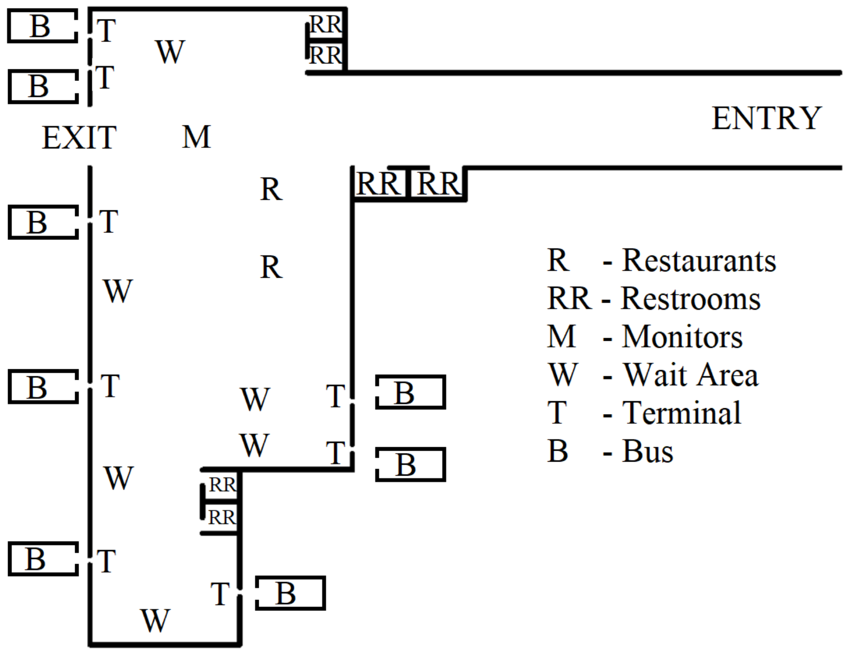

Figure 5.9: A portion of the Hartsfield-Jackson Atlanta International Airport, Atlanta GA.

the population sizes is large, inside the bus the population size for $N = 400$ and 1000 differ only by 10 pedestrians. As the bus population size is larger for $N = 1000$, the average values are higher than that of $N = 400$ for the same number of primaries.

5.3.3 Arriving at a New Airport

As stated earlier, we want to trace the disease spread caused by a sick person who boards a flight in an airport and have a transit connection in another to reach their final destination. We consider the case where buses are not part of the domain and also the case where they are. We track the sick person only inside the airports and the buses. Houston's Hobby airport simulation covered the first part of the journey. Now, we consider a new airport for their remaining journey. In this section, we choose

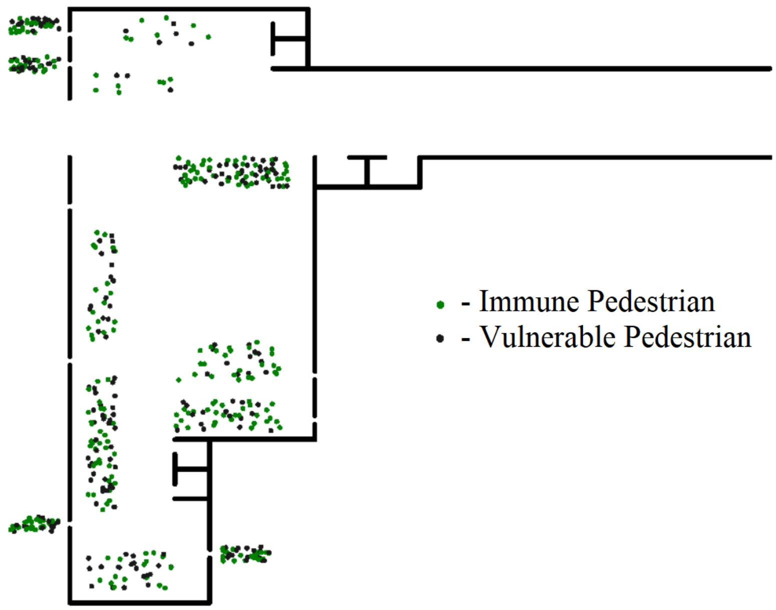

Figure 5.10: Screenshot of the Atlanta airport at the start of the simulation. Pedestrians are represented with a • and each color represents the different stages (immune, vulnerable).

our primary contacts to have a path thats starts inside a bus, move into the airport via terminal exit and eventually board another plane by taking a bus.

A small portion of the Hartsfield-Jackson Atlanta International Airport, Atlanta GA is taken as the new domain. The dimensions are taken from Google Maps. Fig. 5.9 shows us the map of the airport. Some people enter through the entry corridor and board the flight - see Fig. 5.11. Some start their path from the wait areas or restaurants inside the airport and eventually board their flights - see Fig. 5.10. Others enter the airport through the terminals from the buses. 10% of such people move on to board their next flight in the same airport. The rest eventually exit the airport. All pedestrians in the system have the options to visit the restrooms and restaurants on their way to board a plane or exit the airport. All terminals are set up to take

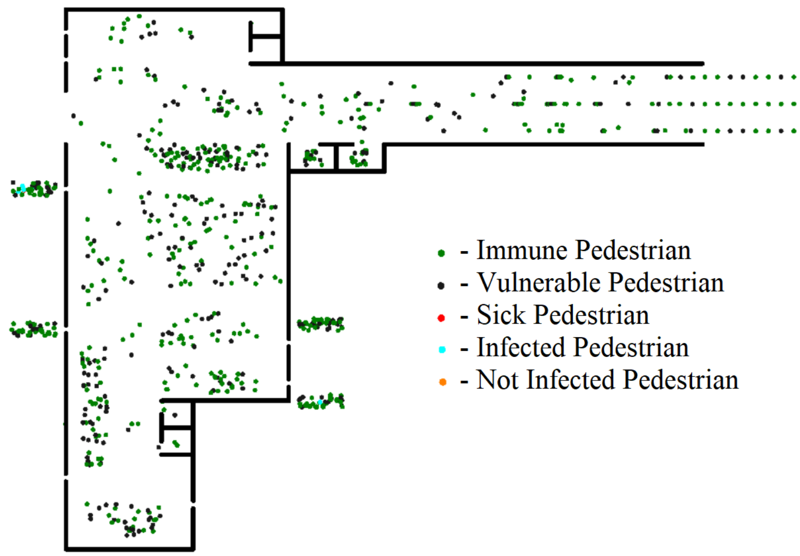

Figure 5.11: Screenshot of the Atlanta airport 20 minutes into the simulation. Pedestrians are represented with a • and each color represents the different stages (immune, vulnerable, sick, infected and not infected).

both incoming (people who board the plane) and outgoing(people who deplane) flow of pedestrians.

Fig. 5.10 shows the airport at the start of a simulation. We can see that 4 buses are filled with pedestrians near the terminals. These pedestrians would spend 5 minutes inside the bus before they start to exit the bus. We also see some pedestrians already inside the airport. These people are waiting to board their planes. The rest of the pedestrians will enter the airport later as per their assigned arrival time (if deplaning) or 15 minutes into the simulation (if entering the airport through the entry corridor). This is seen in Fig. 5.11. Note that in Fig. 5.10, there are no sick people initially. In this scenario, they are assigned to arrive at the airport at a later time.

As before, the microscopic dynamics model parameters are set as: $dt = 0.01$ s, $\tau = 0.5$ s, $\tau_d = 0.18$ s, $r_p = r_w = 2$ m, $d_i^0 = 0.20$ m, and $\mu = \mu_w = 0.3$. The contact tracking model parameters are set as: The cut-off radius $r_s = 2.5$ m and the probability of getting infected, if vulnerable, $v_s = 90\%$. Each of the cases that follow vary the values of $P_{imm} = 90\%, 80\%, 70\%, 60\%$ for each of their run. Each experiment (4 in total) is run 200 times to calculate Avg_{sc} - the average number of secondary contacts yielded.

The two cases we consider now differ only in the number of primary contacts:

Case 1: We start by setting the number of pedestrians $N = 1000$, the total time of the simulation $T = 50$ minutes and the amount of time to potentially get infected $t_v = 2$ minute. We also set the number of primary contacts to be 1.

Case 2: We set $N = 1000$, $T = 50$ minutes and $t_v = 2$ minutes and the number of primary contacts to be 2.

The right plot in Fig. 5.12 provides us with the average number of secondary contacts for case 1 and 2. It shows that the larger the number of primaries, higher the increase in Avg_{sc}, as is trivial. The left plot in Fig. 5.12 contains data extracted from the simulations run. It shows the average number of pedestrians infected inside the airport only, i.e. without buses. Comparing the plots in Fig. 5.12, we can see that having buses as part of the domain produces more than double the number of secondary contacts produced with no buses.

Fig. 5.13 displays the average number of secondary contacts produced for $N = 1000$ pedestrians, in specific locations (only in buses / only inside airports). This data was also extracted from the simulations with buses. In Fig. 5.13, consider the Avg_{sc} values in the case with 1 primary, domain only buses and the ones in the case with 2 primaries, domain only inside airport. They are in close proximity to each other, implying that being in a high density area like a bus drastically increases the rate of increase in Avg_{sc}.

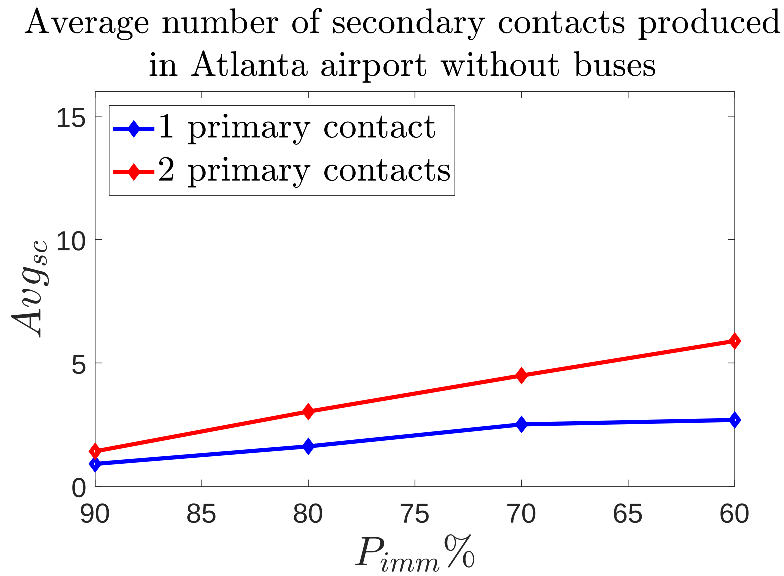

(a) Without buses.

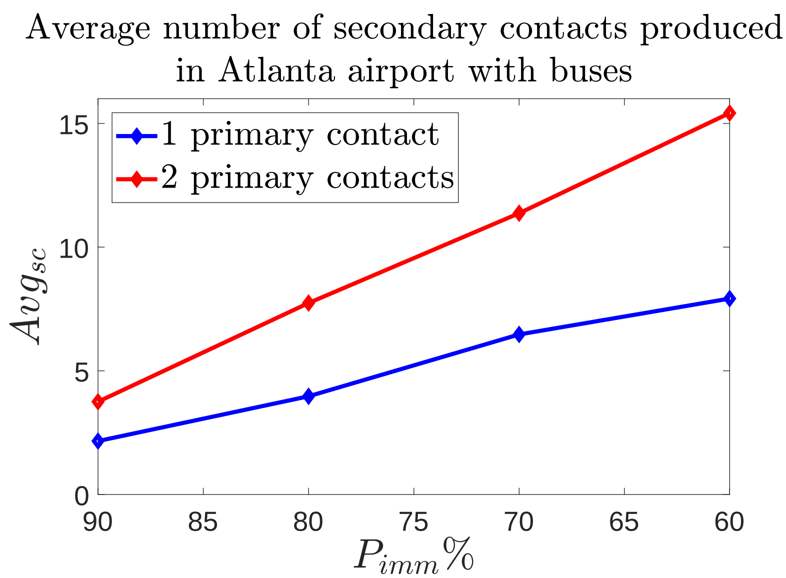

(b) With buses.

Figure 5.12: Average number of secondary contacts produced for $N = 1000$ pedestrians for different P_{imm} in Atlanta airport without and with buses.

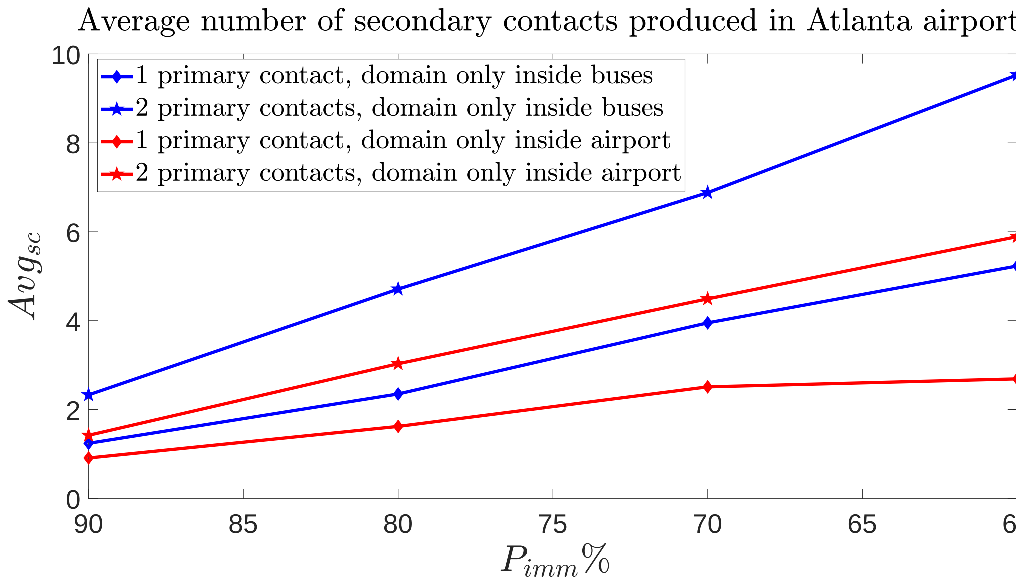

Figure 5.13: Average number of secondary contacts produced for $N = 1000$ pedestrians for different P_{imm} in Atlanta airport, in specific locations (only inside buses / only inside airports).

5.3.4 Conclusion

In this section, our main focus was to track the average number of secondary contacts induced by small number of primaries involving medium size population with immune and vulnerable people in airports. We chose to track sick people who travel through two airports to reach their final destination. We coupled the pedestrian motion dynamics used in Chapter 2 with the contact tracking model in this chapter to simulate this scenario. The results from one airport were consistent with the results from the other. We concluded in the case with airports without buses that:

- For same size populations, an increase in primaries causes an increase in the average number of infected pedestrians.

- The larger the population size, the higher the rate of increase in the average

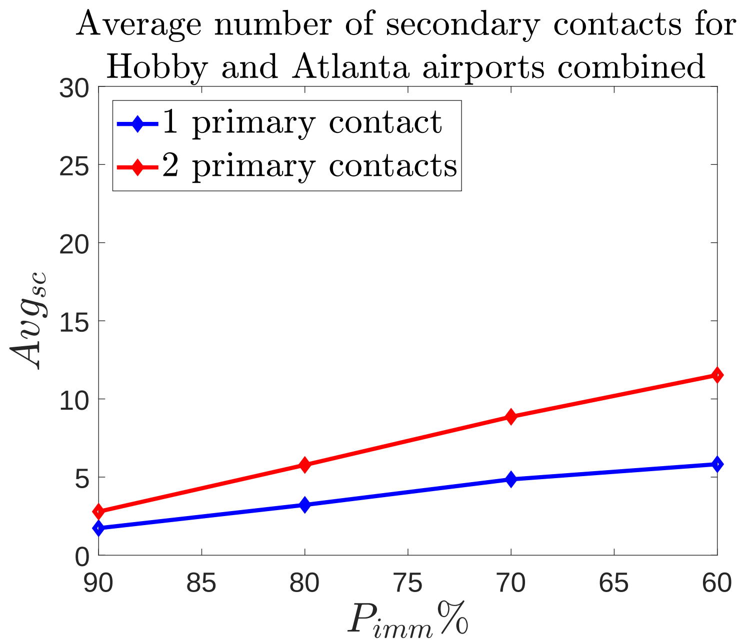

(a) Without buses.

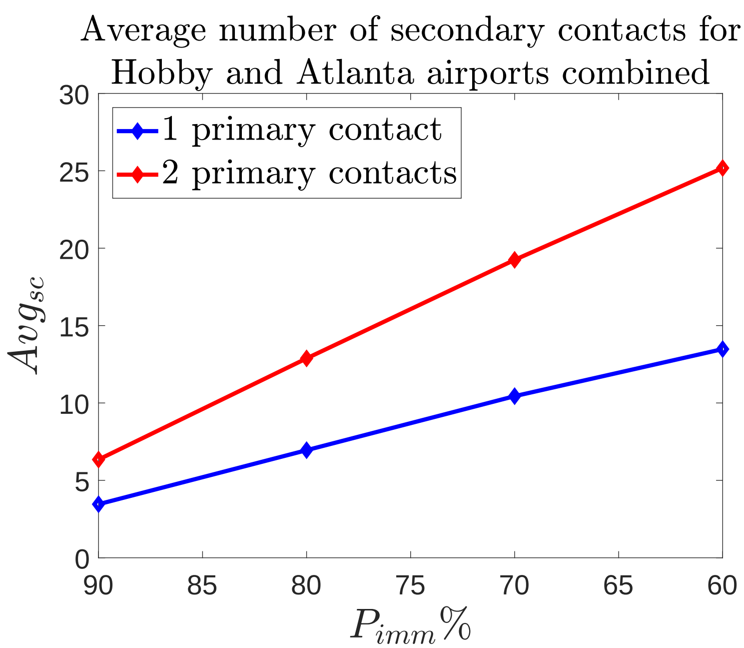

(b) With buses.

Figure 5.14: Average number of secondary contacts produced for $N = 1000$ pedestrians for different P_{imm}, in both Hobby and Atlanta airports combined.

number of infected pedestrians.

- As the population size increases, the number of secondary contacts increases.

In the case of airports with buses we further concluded that having people board a bus to reach the planes were a costly mistake in prevention of the spread of the disease. Being a high density area, buses drastically increased the rate at which people were getting infected. Fig. 5.14 shows the combined average number of secondary contacts produced by sick people who boarded a flight in Hobby and had a transit connection in Atlanta on the way to their final destination. Clearly, having a high percentage of immune pedestrians in the system help in making sure the number of infected people remain small. Also, smaller number of primary contacts, shorter time spent in the airport, lower density of people in the airport and not having buses contribute to reduced number of secondary contacts.

Chapter 6

Conclusion

In this dissertation we analyzed the numerical results of a microscopic approach to modeling pedestrian dynamics.

We first set up a grid free microscopic model for pedestrian dynamics using Newton's second law of motion. Pedestrians are modeled as circles with forces acting on them. The three forces acting on a person are considered to be the target force, the interaction forces between their neighboring pedestrians and the interaction forces between walls or other obstacles near them. The model results in a high dimensional system of second order ordinary differential equations. We studied the sensitivity of the model to every model parameter to see its effect on the pedestrian dynamics. A pedestrian exceeding their desired speed is a very good indicator of the system becoming unstable. Thus we analyzed each parameter by varying it in a series of experiments and observing the speed of a random pedestrian. The overlaps and oscillations in the system (common in force based models) were quantified and studied by varying the interaction constant.

Once the calibration of the model was done, we proceeded to validate it. Numerical results from a kinetic theory approach in [1] were compared with our microscopic model. Evacuation times were computed for varying exit door size of a square room. Our model produced a similar evacuation time curve to that of the kinetic model but had a higher rate of decrease of the evacuation time. Then we compared our numerical results with the empirical results data from [59]. We considered a group of people passing through a corridor. The macroscopic quantities such as flux, density and average velocity were computed for a reference line in the corridor. The numerical results were in good agreement with the empirical data. Finally, we observed a self organizing phenomenon, i.e. lane formation in our model for bidirectional flow of pedestrians in a corridor. We also noticed that the density and initial positioning of the pedestrians played central roles in the number of lanes formed inside the corridor. These validation steps show that the model is adept at simulating pedestrian motion.

Lastly, we added a contact tracking model to the existing microscopic model to compute the number of people who could get infected (through air) by sick people around them. We considered that a vulnerable person could potentially get infected if around a sick person for a considerable amount of time. We computed the average number of secondary contacts produced in the case of sick people going to an airport, boarding a plane and reaching their destination through a transit airport. We also considered the case where people could board a bus to reach their planes. Sick people were traced only when inside airports or buses. We concluded that higher percentage of immune pedestrians, smaller number of primary contacts, shorter time spent in the airport, lower density of people in the airport and not having buses contributed to reduced number of secondary contacts.

6.0.1 Future work

In the specific domain of disease spreading in airports, we can simulate different airport structures and flight boarding systems to come up with best practices that can help reduce disease spread. For instance, it will help to know if confining passengers to the area around gates long before departure can contribute to a reduced rate of infection.

Our focus thus far has been on modeling spreading of diseases in airports. A natural extension of this would be to expand or change the domain under consideration - such as inside airplanes, hospital emergency rooms and even entire communities. Another possible extension is to widen the network of airports visited by sick people and track disease spread across them. It would also be useful to understand spreading behavior of particular diseases, in order to come up with specific mitigation plans. This can be done by fine tuning the model with disease-specific features.

Bibliography

[1] J. P. Agnelli, F. Colasuonno, and D. Knopoff. A kinetic theory approach to the dynamics of crowd evacuation from bounded domains. *Mathematical Models and Methods in Applied Sciences*, 25(01):109–129, 2015.

[2] Gianluca Antonini, Michel Bierlaire, and Mats Weber. Discrete choice models of pedestrian walking behavior. *Transportation Research Part B: Methodological*, 40(8):667 – 687, 2006.

[3] Maia Martcheva Carlos Castillo-Chvez Anuj Mubayi, Christopher Kribs Zaleta. A cost-based comparison of quarantine strategies for new emerging diseases. *Mathematical Biosciences and Engineering*, 7(1551-0018-2010-3-687):687, 2010.

[4] Miho Asano, Takamasa Iryo, and Masao Kuwahara. Microscopic pedestrian simulation model combined with a tactical model for route choice behaviour. *Transportation Research Part C: Emerging Technologies*, 18(6):842 – 855, 2010. Special issue on Transportation Simulation Advances in Air Transportation Research.

[5] Frank G. Ball, Edward S. Knock, and Philip D. O'Neill. Threshold behaviour of emerging epidemics featuring contact tracing. *Advances in Applied Probability*, 43(4):1048–1065, 2011.

[6] Stefania Bandini, Sara Manzoni, and Giuseppe Vizzari. Agent based modeling and simulation: An informatics perspective. *Journal of Artificial Societies and Social Simulation*, 12(4):4, 2009.

[7] N. Bellomo, D. Knopoff, and J. Soler. On the difficult interplay between life, "complexity";, and mathematical sciences. *Mathematical Models and Methods in Applied Sciences*, 23(10):1861–1913, 2013.

[8] N. Bellomo, B. Piccoli, and A. Tosin. Modeling crowd dynamics from a complex system viewpoint. *Mathematical Models and Methods in Applied Sciences*, 22(supp02):1230004, 2012.

[9] Nicola Bellomo and Abdelghani Bellouquid. On the modeling of crowd dynamics: Looking at the beautiful shapes of swarms. *Networks and Heterogeneous Media*, 6(3):383–399, 2011.

[10] Nicola Bellomo and Christian Dogbe. On the modeling of traffic and crowds: A survey of models, speculations, and perspectives. *SIAM Review*, 53(3):409–463, 2011.

[11] Victor Blue and J.L. Adler. pages 293–312, 01 2000.

[12] Victor Blue and Jeffrey L. Adler. Cellular automata microsimulation of bidirectional pedestrian flows. 1678:135–141, 11 1999.

[13] C Burstedde, K Klauck, A Schadschneider, and J Zittartz. Simulation of pedestrian dynamics using a two-dimensional cellular automaton. *Physica A: Statistical Mechanics and its Applications*, 295(3):507 – 525, 2001.

[14] Glenn Webb Cameron Browne, Hayriye Gulbudak. Modeling contact tracing in outbreaks with application to ebola. *Journal of Theoretical Biology*, 384:33–49, 2015.

[15] Nitish Chooramun, Peter J. Lawrence, and Edwin R. Galea. An agent based evacuation model utilising hybrid space discretisation. *Safety Science*, 50(8):1685 – 1694, 2012. Evacuation and Pedestrian Dynamics.

[16] M. Chraibi, A. Seyfried, A. Schadschneider, and W. Mackens. Quantitative description of pedestrian dynamics with a force-based model. In *IEEE/WIC/ACM International Joint Conference on Web Intelligence and Intelligent Agent Technology IEEE Computer Society, Los Alamitos, CA*, volume 3, pages 583–586, 2009.

[17] Mohcine Chraibi, Ulrich Kemloh, Andreas Schadschneider, and Armin Seyfried. Force-based models of pedestrian dynamics. *Networks and Heterogeneous Media*, 6(3):425–442, 2011.

[18] Mohcine Chraibi, Armin Seyfried, and Andreas Schadschneider. Generalized centrifugal-force model for pedestrian dynamics. *Phys. Rev. E*, 82:046111, Oct 2010.

[19] Jicai Dai, Xia Li, and Lin Liu. Simulation of pedestrian counter flow through bottlenecks by using an agent-based model. *Physica A: Statistical Mechanics and its Applications*, 392(9):2202 – 2211, 2013.

[20] Jan Dijkstra, Joran Jessurun, H.J.P. Timmermans, A J Jessurun@tue, Nl , and H J P Timmermans@tue. 01 2001.

[21] Schafer IJ Dixon MG. Ebola viral disease outbreak–west africa, 2014. *Centers for Disease Control and Prevention (CDC), MMWR Morb Mortal Wkly Rep.*, 63(25):548–551, 2014.

[22] Martin Eichner. Case isolation and contact tracing can prevent the spread of smallpox. *American Journal of Epidemiology*, 158:118128, 2003.

[23] Bo Einarsson, editor. *Accuracy and Reliability in Scientific Computing*. Software, Environments and Tools. SIAM, Linköping University, Linköping, Sweden, 2005.

[24] Anderson R.M Ferguson N.M Fraser C, Riley S. Factors that make an infectious disease outbreak controllable. *Proc. Natl Acad. Sci. USA*, 101:61466151, 2004.

[25] Anderson R.M Garnett G.P. Sexually transmitted diseases and sexual behavior: insights from mathematical models. *J. Infect. Dis.*, 174:S150S161, 1996.

[26] Ajelli Marco Yang Zhenhua Mukasa LeonardN. Patil-Naveen Kirschner DeniseE. Merler Stefano Guzzetta, Giorgio. Effectiveness of contact investigations for tuberculosis control in arkansas. *Journal of Theoretical Biology*, 380:238246, 2015.

[27] B. D. Hankin and R. A. Wright. Passenger flow in subways. *OR*, 9(2):81–88, 1958.

[28] Dirk Helbing. A mathematical model for the behavior of pedestrians. *Behavioral Science*, 36(4):298–310, 1991.

[29] Dirk Helbing. Collective phenomena and states in traffic and self-driven many-particle systems. *Computational Materials Science*, 30(12):180 – 187, 2004. Selected papers of the Twelfth International Workshop on Computational Materials Science (CMS2002).

[30] Dirk Helbing, Ills Farkas, Peter Molnar, and Tams Vicsek. Simulation of pedestrian crowds in normal and evacuation situations. 21:21–58, 01 2002.

[31] Dirk Helbing and Péter Molnár. Social force model for pedestrian dynamics. *Phys. Rev. E*, 51:4282–4286, May 1995.

[32] Dirk Helbing and Tamas Vicsek. Optimal self-organization. *New Journal of Physics*, 1(1):13, 1999.

[33] Yorke J.A Hethcote H.W. Gonorrhea transmission dynamics and control. *Springer Lecture Notes in Biomathematics, Berlin:Springer*, 1984.

[34] Roger L. Hughes. A continuum theory for the flow of pedestrians. *Transportation Research Part B: Methodological*, 36(6):507 – 535, 2002.

[35] Li Jia AnnStanley E. Hyman, JamesM. Modeling the impact of random screening and contact tracing in reducing the spread of hiv. 181.

[36] Rowland R Kao Istvan Z Kiss, Darren M Green. Disease contact tracing in random and clustered networks. *Proceedings of the Royal Society B*, 272:14071414, 2005.

[37] Anders Johansson, Dirk Helbing, and Pradyumn K. Shukla. Specification of the social force pedestrian model by evolutionary adjustment to video tracking data. *Advances in Complex Systems*, 10(supp02):271–288, 2007.

[38] McKendrick A.G Kermack W.O. A contribution to the mathematical theory of epidemics. *Proc. R. Soc.*, 115:700721, 1927.

[39] Don Klinkenberg, Christophe Fraser, and Hans Heesterbeek. The effectiveness of contact tracing in emerging epidemics. *PLOS ONE*, 1(1):1–7, 12 2006.

[40] Taras I. Lakoba, D. J. Kaup, and Neal M. Finkelstein. Modifications of the helbing-molnr-farkas-vicsek social force model for pedestrian evolution. *SIMULATION*, 81(5):339–352, 2005.

[41] S. Liu, S. Lo, J. Ma, and W. Wang. An agent-based microscopic pedestrian flow simulation model for pedestrian traffic problems. *IEEE Transactions on Intelligent Transportation Systems*, 15(3):992–1001, June 2014.

[42] Shaobo Liu, Lizhong Yang, Tingyong Fang, and Jian Li. Evacuation from a classroom considering the occupant density around exits. *Physica A: Statistical Mechanics and its Applications*, 388(9):1921 – 1928, 2009.

[43] Jian Ma, Wei guo Song, Jun Zhang, Siu ming Lo, and Guang xuan Liao. k-nearest-neighbor interaction induced self-organized pedestrian counter flow. *Physica A: Statistical Mechanics and its Applications*, 389(10):2101 – 2117, 2010.

[44] Kretzschmar Mirjam Dietz Klaus Mller, Johannes. Contact tracing in stochastic and deterministic epidemic models. *Mathematical Biosciences*, 164:39–64, 2000.

[45] Mehdi Moussaïd, Dirk Helbing, Simon Garnier, Anders Johansson, Maud Combe, and Guy Theraulaz. Experimental study of the behavioural mechanisms underlying self-organization in human crowds. *Proceedings of the Royal Society of London B: Biological Sciences*, 276(1668):2755–2762, 2009.

[46] D.R. Parisi and C.O. Dorso. Morphological and dynamical aspects of the room evacuation process. *Physica A: Statistical Mechanics and its Applications*, 385(1):343 – 355, 2007.

[47] Lofgren E.T. Marathe M. Eubank S. Lewis-B.L. Rivers, C.M. Modeling the impact of interventions on an epidemic of ebola in sierra leone and liberia. *PLoS Curr.,6*, 2014.

[48] Grenfell B.T Rohani P, Earn D.J.D. The impact of immunisation on pertussis transmission in england and wales. *Lancet*, 355:285286, 2000.

[49] Andreas Schadschneider, Wolfram Klingsch, Hubert Klüpfel, Tobias Kretz, Christian Rogsch, and Armin Seyfried. *Evacuation Dynamics: Empirical Results, Modeling and Applications*, pages 517–550. Springer New York, New York, NY, 2011.

[50] Armin Seyfried, Oliver Passon, Bernhard Steffen, Maik Boltes, Tobias Rupprecht, and Wolfram Klingsch. New insights into pedestrian flow through bottlenecks. *Transportation Science*, 43(3):395–406, 2009.

[51] A. Shende, M. P. Singh, and P. Kachroo. Optimization-based feedback control for pedestrian evacuation from an exit corridor. *IEEE Transactions on Intelligent Transportation Systems*, 12(4):1167–1176, Dec 2011.

[52] Musa EO et al Shuaib F, Gunnala R. Ebola virus disease outbreak - nigeria, july-september 2014. *Centers for Disease Control and Prevention (CDC), MMWR Morb Mortal Wkly Rep.*, 63(39):867872, 2014.

[53] Yusuke Tajima, Kouhei Takimoto, and Takashi Nagatani. Pattern formation and jamming transition in pedestrian counter flow. *Physica A: Statistical Mechanics and its Applications*, 313(3):709 – 723, 2002.

[54] Alasdair Turner and Alan Penn. Encoding natural movement as an agent-based system: An investigation into human pedestrian behaviour in the built environment. *Environment and Planning B: Planning and Design*, 29(4):473–490, 2002.

[55] Jonathan A. Ward, Andrew J. Evans, and Nicolas S. Malleson. Dynamic calibration of agent-based models using data assimilation. *Royal Society Open Science*, 3(4), 2016.

[56] Xingang Li Xiaomeng Li, Xuedong Yan and Jiangfeng Wang. Using cellular automata to investigate pedestrian conflicts with vehicles in crosswalk at signalized intersection. page 16, 10 2012.

[57] S. Xu and H. B. L. Duh. A simulation of bonding effects and their impacts on pedestrian dynamics. *IEEE Transactions on Intelligent Transportation Systems*, 11(1):153–161, March 2010.

[58] W. J. Yu, R. Chen, L. Y. Dong, and S. Q. Dai. Centrifugal force model for pedestrian dynamics. *Phys. Rev. E*, 72:026112, Aug 2005.

[59] J. Zhang, W. Klingsch, A. Schadschneider, and A. Seyfried. Transitions in pedestrian fundamental diagrams of straight corridors and t-junctions. *J. Stat. Mech.*, 2011:P06004, 2011.

[60] B. Zhou, X. Wang, and X. Tang. Understanding collective crowd behaviors: Learning a mixture model of dynamic pedestrian-agents. In *2012 IEEE Conference on Computer Vision and Pattern Recognition*, pages 2871–2878, June 2012.